Internal Condensing Flows inside a Vertical Pipe: Experimental/ Computational Investigations of the Effects of Specified and Unspecified (Free) Conditions at Exit

A. Narain[1]
Fellow ASME
e-mail: narain@mtu.edu

J. H. Kurita

M. Kivisalu

A. Siemionko

S. Kulkarni

T. W. Ng

N. Kim

L. Phan

Department of Mechanical Engineering-Engineering Mechanics,
Michigan Technological University,
Houghton, MI 49931

Reported experimental and computational results confirm that both the flow features and heat-transfer rates inside a condenser depend on the specification of inlet, wall, and exit conditions. The results show that the commonly occurring condensing flows' special sensitivity to changes in exit conditions (i.e., changes in exit pressure) arises from the ease with which these changes alter the vapor flow field in the interior. When, at a fixed steady mass flow rate, the exit pressure is changed from one steady value to another, the changes required of the interior vapor flow toward achieving a new steady duct flow are such that they do not demand a removal of the new exit pressure imposition back to the original steady value—as is the case for incompressible single phase duct flows with an original and "required" exit pressure. Instead, new steady flows may be achieved through appropriate changes in the vapor/liquid interfacial configurations and associated changes in interfacial mass, heat-transfer rates (both local and overall), and other flow variables. This special feature of these flows has been investigated here for the commonly occurring large heat sink situations, for which the condensing surface temperature (not heat flux) remains approximately the same for any given set of inlet conditions while the exit-condition changes. In this paper's context of flows of a pure vapor that experience film condensation on the inside walls of a vertical tube, the reported results provide an important quantitative and qualitative understanding and support an exit-condition-based categorization of the flows. Experimental results and selected relevant computational results that are presented here reinforce the fact that there exist multiple steady solutions (with different heat-transfer rates) for multiple steady prescriptions of the exit condition—even though the other boundary conditions do not change. However, for some situations that do not fix any specific value for the exit condition (say, exit pressure) but allow the flow the freedom to choose any exit pressure value within a certain range, experiments confirm the computational results that, given enough time, there typically exists, under normal gravity conditions, a self-selected "natural" steady flow with a natural exit condition. This happens if the vapor flow is seeking (or is attracted to) a specific exit condition and the conditions downstream of the condenser allow the vapor flow a range of exit conditions that includes the specific natural exit condition of choice. However, for some unspecified exit-condition cases involving partial condensation, even if computations predict that a natural exit-condition choice exists, the experimental arrangement employed here does not allow the flow to approach its steady natural exit-condition value. Instead, it only allows oscillatory exit conditions leading to an oscillatory flow. For the reported experiments, these oscillatory pressures are induced and imposed by the instabilities in the system components downstream of the condenser.
[DOI: 10.1115/1.2755063]

Keywords: film condensation, phase-change heat transfer, two-phase flows, interfacial waves

1 Introduction and Background

This paper outlines a fundamental and novel experimental investigation of effects of exit conditions on internal condensing flows. Reported experimental results confirm the existing computational results [1–3] that both the flow features and heat-transfer rates inside a condenser are sensitive to exit conditions and therefore depend on the specification of inlet, wall (particularly condensing surface temperature), and exit conditions. The condensing surface temperature (not heat flux) is assumed to be known (and fixed) or knowable (through consideration of the appropriate conjugate problem). This is true because, geneally, heat is removed from the condensing flow through a wall and put in a large heat sink, which may be a steady coolant flow in contact with the other

[1]Corresponding author.

Contributed by the Heat Transfer Division of ASME for publication in the JOURNAL OF HEAT TRANSFER. Manuscript received October 18, 2005; final manuscript received February 10, 2007. Review conducted by Ramendra P. Roy. Paper presented at the 2005 ASME International Mechanical Engineering Congress (IMECE2005), Orlando, FL, November 5, 2005.

side of the wall surface or a suitabe arrangement of thermoelectric coolers. This paper identifies and establishes a multiplicity of steady/quasisteady solutions—and/or oscillatory flows—under different conditions at the exit. Experiments support the existing simulation results [1–3] that have already shown, among other results, the presence of different steady/quasisteady solutions for different steady specifications of the exit condition. The condenser exit condition (for partial as well as full condensation (FC)) is specified by the exit pressure. For partial (incomplete) condensation flows, the specification of the exit pressure is equivalent (see Fig. 6 in Ref. [1]) to the specification of the exit vapor quality, i.e., the ratio of the vapor mass flow rate at the exit to the inlet mass flow rate (see simulation results from Refs. [1–3]). The computational simulations [1–3] for the gravity driven partial condensation cases (such as flows inside a vertical tube) also predict that for a certain set of inlet and wall conditions, even if the exit condition is not specified and a suitable range of exit conditions is available for the flow to choose from, the flow seeks and attains a specific "natural" exit condition (in Narain et al. [1], this situation is also termed natural unspecified steady exit condition due to the presence of an "attractor," i.e., an "attracting" solution). Unfortunately, many planned system designs incorporate a condenser and assume that the condenser will *always* attain a steady flow even if no exit conditions are specified. This is not generally true. The attainment of natural steady flows under unspecified exit conditions occurs more readily (over a larger parameter zone) for gravity driven condensate flows as opposed to shear driven flows (see Ref. [3]). The reported experimental results for gravity driven partial condensation cases under unspecified exit conditions support the computational results—both qualitatively and quantitatively. However, a steady natural exit condition may or may not exist depending on whether or not a steady attractor exists (e.g., as shown in Ref. [3], it does not exist for most slow inlet flow rates in horizontal or zero gravity conditions), and even if an attractor does exist, its realization depends on whether the attracting natural exit-condition value falls within the range of the available steady choices at the exit. In the absence of an *active* specification of a steady exit condition, the available range of steady exit conditions is determined by the components downstream of the condenser as well as the specific nature of the hardware used in the design of the rest of the system (or flow loop). Furthermore, because of the small pressure drops (see Ref. [3] or experimental runs reported here), when a steady natural exit condition is achieved under unspecified conditions or when the specified exit condition is not too far from this natural steady exit value, typically, vapor flows are close to incompressible.

The fact that for partial condensation flows, one can achieve quite different values of average heat-transfer coeffiecients under different realizations of quasisteady flows that correspond to different specifications of exit vapor quality (or pressure) is not surprising—as this follows from a simple overall energy balance. In the context of *boundary value* problems for internal condensing flows, what is new is that our computational and experimental results unequivocally show that the commonly occurring condensing flows are very sensitive to the nature of exit conditions as well as to the changes in exit conditions (due to changes in exit pressure). This sensitivity arises from the ease with which these changes alter the vapor flow field in the interior. Therefore, when only the exit condition is changed from one steady value to another, the changes required for the interior vapor flow toward attaining a new steady flow are such that they do not demand a removal of the new exit pressure imposition—as is the case for incompressible single phase duct flows with only one allowed exit pressure. Instead, for condensing flows, new steady flows are achieved for new exit conditions through appropriate changes in the vapor/liquid interfacial configurations and associated changes in interfacial mass, heat-transfer rates (both local and overall), and other flow variables.

The vertical in-tube internal condensing flows—partial or complete (full)—are investigated here for a downflow configuration. Though numerous in-tube condensation experiments have been done, most of the well-known in-tube vertical downflow experiments done by Goodykoontz and Dorsch [4,5], Carpenter [6], etc., either limited themselves to sufficiently fast flow portions of the duct that do not significantly depend on exit conditions or operated under a particular (natural or otherwise) set of exit conditions (that gets specified or remains unspecified depending on the employed experimental setup). Therefore, results may vary from one experimental system to another. In addition to our group's very early (see Yu [7]) and subsequent [1,2] computational findings on the importance of exit conditions for internal condensing flows, experimental findings of Rabas and Arman [8] also indicated the significance of exit conditions through their observation that the presence or absence of valves at the exit affected some of their in-tube vertical downflow results. Rabas and Arman [8] also pointed out an important fact that in the annular regime, even for a complete condensation vertically downward flow inside a tube (for which, at exit, the condensate is collected in a vapor plenum), the condensing flow is usually annular not only all the way up to the point of FC but also downstream of this point up to the exit; that is, a continuous liquid phase never fills the entire tube. This means that the flow remains annular (or, at most, has a few liquid bridges that encapsulate vapor bubbles) with zero interfacial mass and heat transfer in the segment downstream of the point of FC. Additionally, Rabas and Arman [8] pointed out that in the case of a horizontal in-tube complete condensation for a tube of a certain diameter, the flow regime near downstream and upstream locations of the point of complete condensation (where vapor flow rate is nearly zero) varies from gravity dominated stratified to gravity dominated plug annular—depending on whether the inlet mass flow rate is above or below a certain critical value.

Furthermore, several experimental results and analyses [9–17] indicate that, for certain physical arrangements leading to a specific class of inlet and outlet conditions, transients and instabilities are expected in complete condensation horizontal in-tube internal condensing flows. Since these experiments and the corresponding modeling techniques in the literature [9–17] limit themselves to a particular type of inlet and exit conditions, they do not directly apply to the presence or absence of observed transients and instabilities in other feasible categories of exit-condition specifications.

Since an understanding of internal condensing flows' transients is not entirely possible in the context of traditional two-phase flow analyses based on homogeneous, separated, or drift-flux formulations (see Wallis [18]), more sophisticated averaged model equations of varying degrees of complexities (see, e.g., Lahey and Drew [19]) have been proposed. Despite this, appropriate drift-flux and/or virtual mass force based analyses of Liao et al. [20], Liao and Wang [21], and Wang [22] reported some ability to capture transients in certain internal condensing flows of the type studied by Wedekind and Bhatt [9,12], Wedekind et al. [15], Bhatt and Wedekind [10,11], Bhatt et al. [13], Kobus et al. [16], Kobus [17], Boyer et al. [14], etc. Furthermore, Liao et al. [20] and Liao and Wang [21] also reported difficulties in employing the multidimensional, four field, two-fluid model of Lahey and Drew [19] toward modeling transients and instabilities that occur in internal condensing flow cases of their concern. Other analyses by Wedekind and Bhatt [9,12], Bhatt and Wedekind [10,11], Kobus et al. [16], and Kobus [17] employed the system mean void fraction (SMVF) model, which allows one to ignore the momentum balance equation. These simpler integral analyses have been somewhat successful in capturing some features of the experimentally observed transients and flow oscillations that have been reported [9,11] for certain in-tube horizontal condensing flows involving a complete condensation. In these cases, a fixed pressure tank (plenum) at a sufficiently high pressure pushes vapor through an inlet valve to the inlet of a horizontal condensing section where the

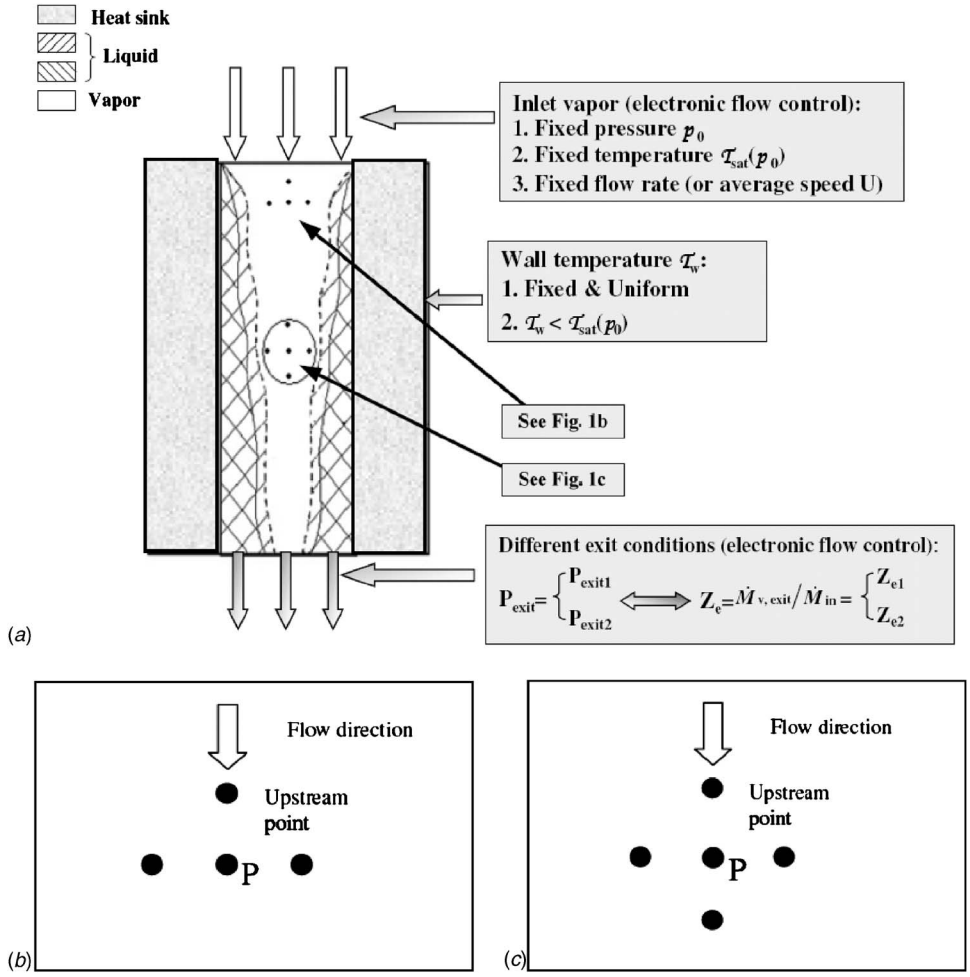

Fig. 1 The schematic for the flow through test-section and exit-condition issues

vapor is fully condensed, and then the liquid flows out of the condenser exit, through an exit valve, to a tank (plenum) at a fixed low pressure.

To understand exit condition issues more clearly, the approach taken here has been to seek an experimental confirmation of key results obtained from employing our fundamental and nearly exact computational technique [1–3] to obtain steady and unsteady simulations for laminar-vapor/laminar-condensate *initial* boundary value problems—in the limited context of separated, quasi-steady annular condensing flows. Therefore, simulation results [1–3] have been central to the development and interpretation of the reported experiments. Fundamentally, the internal condensing flows' exit condition sensitivity arises from governing equations being "elliptic" or requiring "two-way" space coordinates in the flow direction (i.e., the flow variable at a point P is influenced by both upstream and downstream local neighbors, as shown in Fig. 1(*c*)). However, this sensitivity to exit conditions, or a two-way behavior, is special and does not result from the typical "ellipticity" associated with slow flows and flow reversals (which are, as described in Patankar [23], associated with the changes in the sign of local Peclet numbers). In fact, it is found (for simulations in Refs. [1–3]) that even when vapor and liquid flows are unidirectional (or "one way" or "parabolic") due to local Peclet numbers (which appear in local discretization equations for the velocity components—see Eqs. (5.61)–(5.64) in Ref. [23]) being very large (even greater than 50,000 in both x and y directions), the flows exhibit an elliptic or a two-way behavior leading to a sensitivity to exit conditions. This special sensitivity to exit condition is due to the two-way behavior of the vapor pressure fields (reflected, in the context of our computational methodology [1], by the two-way behavior of the pressure equations given by Eqs. (6.30) and (6.31) in Ref. [23]). These equations for condensing flows are such that the coefficients that multiply the pressures at the locally upstream and downstream neighbors are comparable even for large Peclet numbers (see pressure discretization equations for the SIMPLER procedure in Patankar [23]). Due to this, effects of changes in the exit pressure are felt by the entire vapor flow field.

In the literature, condensing flows have been classified according to whether they are shear dominated or gravity dominated, internal or external, smooth or wavy at the interface, laminar or turbulent in the two phases, etc. It is proposed here that one can only make sense of the vast literature on internal condensing flows if they are also classified in different categories based on the conditions imposed at the inlet and the exit. The following three categories (termed categories I–III) proposed here cover most cases of interest.

(1) Category I (with complete or incomplete condensation under *specified* exit conditions)

- Prescribed or known values of the total inlet vapor mass flow rate $\dot{M}_{in}$ (kg/s), inlet vapor quality, inlet pressure p_{in}, and inlet temperature at all times t. Without loss of generality, one can focus on an all vapor flow (an inlet vapor quality of unity) at the inlet with known values of the total inlet (all vapor) mass flow rate $\dot{M}_{in}$ (kg/s), inlet pressure p_{in}, and inlet temperature (at saturation temperature $T_{sat}(p_{in})$ or at some superheat) at all times t. This

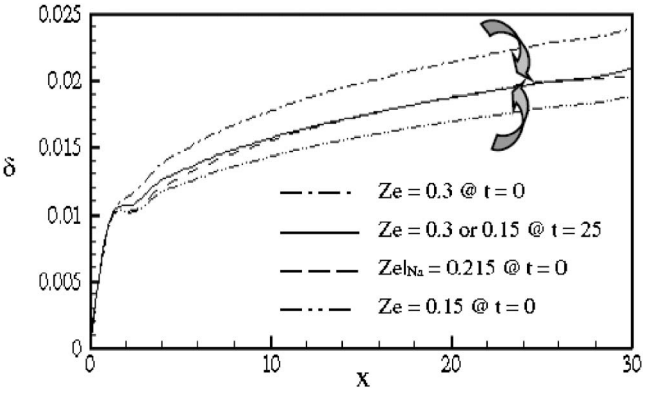

Fig. 2 For tube flow situations specified as in Phan et al. [3] (see their Table 1 and Fig. 2), the figure depicts three steady film thickness profiles for three different exit conditions. The figure also indicates time trends for two sets of $\delta(x,t)$ predictions for $t>0$; one curve starts at $Z_e=0.3$ at $t=0$, and tends, as $t\to\infty$, to the solution for $Z_{e|Na}=0.215$. The other curve starts at $Z_e=0.15$ at $t=0$ and tends, as $t\to\infty$, to the same $Z_{e|Na}=0.215$ solution.

means the prescription could be steady or unsteady.

- Prescribed method of cooling leading to known wall temperatures $T_w(x,t)<T_{sat}(p_{in})$ for all x locations over which film condensation occurs. Typical wall temperature conditions of interest are steady, but unsteady conditions are relevant to start-up and shutdown.
- Specified or known exit condition. For example, for steady exit conditions, the exit pressure p_e, is a const, which is equivalent, for partial condensation cases, to setting exit mass quality $Z_e \equiv \dot{M}_{vapor@exit}$ (kg/s)/ $\dot{M}_{in}$ (kg/s), an appropriate constant where $\dot{M}_{vapor@exit}$ (kg/s) is the vapor mass flow rate at the exit at time t.

  For category I partial condensation flows with steady specified exit conditions, the computational simulations in Fig. 2 (with the flow conditions being the same as specified in Fig. 2 and Table 1 of Phan et al. [3]) show three different steady solutions for three different specified vapor qualities Z_e at the exit (viz., $Z_{e1}=0.15$, $Z_{e2}=0.215$, and $Z_{e3}=0.3$). Some of the experimental investigations of Garimella et al. [24,25] are for flows in this category with an inlet quality $Z_i(<1)$ and an exit quality Z_e specified at values incrementally smaller than Z_i.

(2) Category II (with complete or incomplete condensation under unspecified exit conditions)

- Prescribed or known values of the inlet mass flow rate $\dot{M}_{in}$ (kg/s), inlet pressure p_{in}, and inlet temperature (at saturation temperature $T_{sat}(p_{in})$ or at some superheat) at all times t. Without loss of generality, it is assumed that the flow is all vapor at the inlet.
- Prescribed or known wall temperatures $T_w(x,t)<T_{sat}(p_{in})$ for all x locations over which film condensation occurs.
- Exit condition is not specified. However, due to some system hardware limitations and constraints, if only a range of exit pressure conditions is available to the condenser, we still call a flow in the interior of this range a category II flow. A flow at the boundary of this range is, however, not a category II flow.

  For category II flows, in Fig. 2, it is computationally shown that if exit vapor quality specification constraints at $Z_{e1}=0.15$ or $Z_{e3}=0.3$ are removed at some time ($t=0$)—and subsequently ($t>0$), one does not specify any exit condition or any restrictions on the available range of exit conditions—this particular incomplete condensation flow seeks its own long-term and steady natural exit vapor quality $Z_{e|Na}=Z_{e2}=0.215$ and an associated steady natural flow under incompressible vapor conditions. Other simulations for shear driven flows [3] and some experiments reported here under conditions of restricted available range of exit conditions show that the flow in this category may or may not be able to select a quasi-steady flow with a natural exit condition. This is because the unspecified exit condition (category II) cases, though commonly used in applications, are essentially "ill posed" boundary value problems. Therefore, the existence of steady solutions is at the mercy of other factors (such as whether or not an attracting steady solution exists and, if it does, whether or not downstream conditions are conducive to the attainment of this attracting solution). When natural attractors are weak or do not exist, as is the case for some horizontal and zero gravity condensing flows [3], the concave bowl analogy schematic for attractors given in Fig. 9 of Narain et al. [1] needs to be replaced by a bowl shape, which is either weakly concave or completely flat. Furthermore, for category II flows, in Phan et al. [3], the existence of an attractor leading to a long-term steady exit condition was termed differently—it was called a long-term one-way or parabolic behavior. Similarly, non-existence of an attractor (typically an indicator of flows that lie outside the annular regime and are more complex in the sense that they exhibit certain degrees of randomness or indeterminacy) was termed differently in Ref. [3]—it was called a long-term two-way or elliptic behavior.

(3) Category III (complete condensation involving special specified conditions at the inlet and the exit)

Although, technically, this is a special subcategory of fully condensing category I flows, it is listed separately because it typically requires a different experimental setup and hardware facilities. This class has been extensively investigated in the literature [9–16] for oscillatory and unsteady condensing flows.

- In this case, there is a constant pressure reservoir, with a high pressure $p_{tank\text{-}in}$, that feeds the vapor flow $\dot{M}_{in}(t)$ (at inlet pressure p_{in}, temperature $T_{V\text{-}in}$, and density $\rho_{V\text{-}in}$) into the test section through an inlet valve (with valve coefficient k_i). This requires the inlet pressure p_{in} to satisfy at any time t,

$$p_{in} \cong p_{tank\text{-}in} - k_i \frac{\dot{M}_{in}(t)^2}{\rho_{V-in}}$$

- Also, there is a constant pressure exit tank, with a typically lower pressure $p_{tank\text{-}exit}$ to which the condensate flows through an exit valve of valve coefficient k_e. The exit valve handles an *all liquid* flow because this case is only for complete condensation flows. At the exit of the condenser, the liquid flow rate is $\dot{M}_{exit}$ at any time t, and the liquid density is $\rho_{L\text{-}exit}$. This requires that the test-section exit pressure p_{exit} satisfy at any time t,

$$p_{exit} \cong p_{tank\text{-}exit} + k_e \frac{\dot{M}_{exit}(t)^2}{\rho_{L-exit}}$$

- Prescribed or known *steady* wall temperatures $T_w(x)<T_{sat}(p_{in})$ for all x locations over which film condensation occurs.

The experimental and/or modeling analysis papers of Wedekind and Bhatt [9,12], Bhatt and Wedekind [10,11], Bhatt et al. [13], Kobus et al. [16], Kobus [17], Liao et al. [20], Liao and Wang [21], etc., focused on category III flows for a horizontal condenser.

The experiments and computations in this paper, however, focus only on category I and category II flows. As a result, the flow transients and system instabilities reported in this paper (see Sec. 5), as far as flows within the test section are concerned, are necessarily of different origin. However, at a system level, the experimentally observed flow oscillations' relationship to the better known [11,13] results for category III flows in the downstream auxiliary condenser is also discussed here.

The experimental runs reported here largely involve laminar condensate and turbulent vapor situations with possible vapor compressibility effects for some of the category I flows. Despite this, both qualitative and quantitative comparisons with simulation results based on the laminar-vapor/laminar-condensate methodology given in Refs. [1–3] are possible and are presented here for a feasible subset (within the boundaries for steady annular flows) of experimental runs. This comparison is possible because turbulent vapor often laminarizes in the vicinity of laminar condensate as the condensate is slow and remains laminar approximately up to $\mathrm{Re}_\delta \leqslant 1800$ (see film Reynolds number Re_δ defined in Phan and Narain [26]). Also, for gravity driven condensate cases considered here, the existence of turbulent vapor zones in the core and entrance zone of the condenser has only a minor second order impact on pressure variations in the condenser. The far field vapor turbulence often tends not to be a significant player because the overall flow features (local and average heat-transfer coefficients) are dominated by interfacial mass and heat-transfer rates, which are dominated by the typically laminar nature of the gravity driven condensate flow and the associated laminar nature of vapor flow in the vicinity of the interface. Because of the above, all experimental runs reported here for partial (or incomplete) condensation cases involving laminar condensate show a very good *qualitative* agreement with the simulations as far as the existence of multiple steady solutions for multiple steady exit conditions (category I) and a natural steady solution for the unspecified exit-condition cases (category II) are concerned. The agreement with simulations, with regard to exit vapor quality and general consistency with overall heat-transfer rates, are also *quantitatively* very good for experimental runs that fit the annular flow assumption for the simulations. It should be noted that, additionally, the accuracy of the employed simulation methodology [1–3] and its quantitative compatibility with a different set of experimental runs (Lu and Suryanarayana [27]) for shear dominated category II flows have also been established (see Ref. [2]). Furthermore, computational results for internal condensing flows are obtained from a simulation tool that has a proven ability (see Phan and Narain [26]) to make good quantitative predictions for wave phenomena and their effects on heat-transfer rates for the benchmark classical problem of Nusselt [28].

The experimental investigation of annular complete condensation cases reported here is less complete and limited to natural steady flows in category II. Computational simulations for these cases are also limited because the flow often condenses completely somewhere within the test section, and the current simulation technique can only approximately cover the zone from the inlet to the point of FC. The simulation tool has not yet been enhanced to automatically identify and handle the exit-pressure-sensitive two-phase annular flow zone—with negligible interfacial mass and heat-transfer rates—that occurs between the point of FC (whose location itself depends on the exit pressure) and the exit. The reported experiments cover natural FC cases under unspecified exit conditions. The hardware needed to investigate a complete condensation under specified exit conditions (category I flows as well as category III flows) is being developed as an important ongoing area of research.

Thus far, nonexistent accounting of exit-condition categories and exit-condition sensitivities of internal condensing flows is perhaps one of the reasons for the large uncertainities and deficiencies noted by Palen et al. [29] with regard to the poor usefulness of quantitative information available from existing correlations for heat-transfer coefficients.

The experiments reported here involve a single pure working fluid (viz., FC-72 by 3M Corp.) and focus on inlet mass flow rates that correspond to inlet vapor Reynolds numbers in the range of 10,000–40,000 and vapor to wall temperature differences of $3-60\,^{\circ}\mathrm{C}$ (i.e., $0 \leqslant \mathrm{Ja} \leqslant 0.4$).

2 Experimental Facility

The condenser section, which is of the type shown in Fig. 1(*a*), is typically a part of a closed flow loop. The flow loop, which maintains a steady input pressure (p_{in}) and mass flow rate ($\dot{M}_{\mathrm{in}}$) at the inlet, while maintaining a prescribed steady (and nearly uniform) condensing surface temperature, may be designed to provide different categories of exit conditions. Exit-condition specifications for category I and category II flows defined earlier in Sec. 1 are realized through flow arrangements indicated in Figs. 3 and 4 respectively.

A 0–500 W evaporator/boiler in Figs. 3 and 4 is used to evaporate the working fluid (FC-72). The vapor mass flow rate out of the evaporator, $\dot{M}_{\mathrm{in}}$, is fed into the test section. This mass flow rate is measured by a Coriolis flow meter F_1, and during transients, this value can be controlled by the pneumatically actuated control valve V_1 (shown connected to F_1 in Figs. 3 and 4). Under steady conditions though, the value of $\dot{M}_{\mathrm{in}}$ gets approximately fixed by the net steady electrical heating rate for the evaporator. This is due to the restriction imposed by the evaporator energy balance, viz., $\dot{M}_{\mathrm{in}} \approx \dot{Q}_b / h_{\mathrm{fg}}(p_b)$. Here, $\dot{Q}_b$ is the net heat rate into the evaporator, p_b is the steady evaporator pressure, $T_b \approx T_{\mathrm{sat}}(p_b)$ is the steady evaporator temperature (which is nearly equal to the saturation temperature of the fluid at pressure p_b), and h_{fg} is the heat of vaporization at the liquid/vapor surface pressure p_b in the evaporator. Toward reduction in start-up time to steady state in the evaporator, the liquid flowing in the evaporator is warmed up (between points P′ and B′ in Figs. 3 and 4), so its temperature is nearly equal to the evaporator temperature $T_b \approx T_{\mathrm{sat}}(p_b)$.

The test section is a 0.8 m long, vertical stainless steel (316 SS) tube with 6.6 mm inner diameter and 12.7 mm outer diameter. At the entrance of the test section, the inlet vapor temperature is denoted as $T_{V\text{-in}}$, the inlet pressure is denoted as p_{in}, and the inlet vapor is kept slightly superheated ($2-10\,^{\circ}\mathrm{C}$ superheat obtained by heating a relevant portion of connecting tubes by a rope heater). A suitable thermocouple and an absolute pressure transducer measure the temperature $T_{V\text{-in}}$ and pressure p_{in}, respectively, of the vapor at the inlet. The dynamic view from an axial boroscope, mounted at the top of the test section shown in Fig. 5, is used to visualize and ascertain the nature of the flow in the first half of the test section. However, because of sharpness and contrast improvements that are needed for better quality images, snapshots and video clips of the flows are not currently included in this paper. They are, however, expected to be available in the near future. We are currently able to use these views to ascertain whether or not annular film condensation begins near the indicated "start of condensation" point in Fig. 5 and to ascertain (and then to ensure) the dryness of the vapor up to the test-section inlet.

The test section (see Fig. 5) is suitably instrumented with various sensors (thermocouples, pressure transducers, etc.). For future work, there is an arrangement to obtain local film thickness data through integration of our recently invented nonintrusive film thickness sensors that utilize the principle of fluorescence and fiber-optic technology (see Ng [30]) and are able to measure the

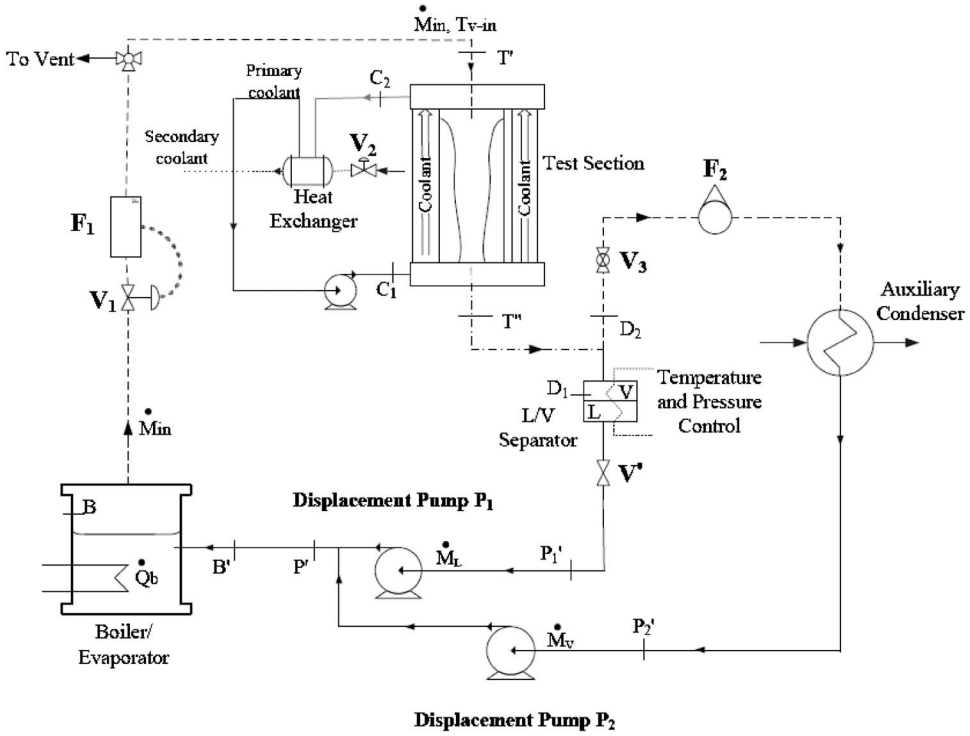

Fig. 3 The schematic of the flow loop for achieving specified exit-condition category I flows for partial condensation cases

"local" time-varying thickness of dynamic liquid films. The technique used for mounting all the sensors is described in detail in Narain et al. [31] and Siemionko [32].

The test section in Fig. 5(*b*) (not shown to scale relative to the outer tube in Fig. 5(*a*)) is centrally aligned in the hollow space of a larger diameter stainless steel (314 SS) tube. This outer tube has an inner diameter of 23.62 mm and an outer diameter of 25.40 mm. The test-section tube is cooled by the flow of cooler water in the annulus formed by the outer surface of the test-section tube and the inner surface of the outer tube. As shown in Figs. 3 and 4, the flow of coolant water is arranged by a separate closed loop consisting of the shell side of the shell-in-tube heat exchanger (the flow is on shell side) and a pump. A separate loop, not shown in Figs. 3 and 4, assures a secondary coolant (cold-water) flow at a steady constant temperature and a steady flow rate through the tube side of the heat exchanger in Figs. 3 and 4. This

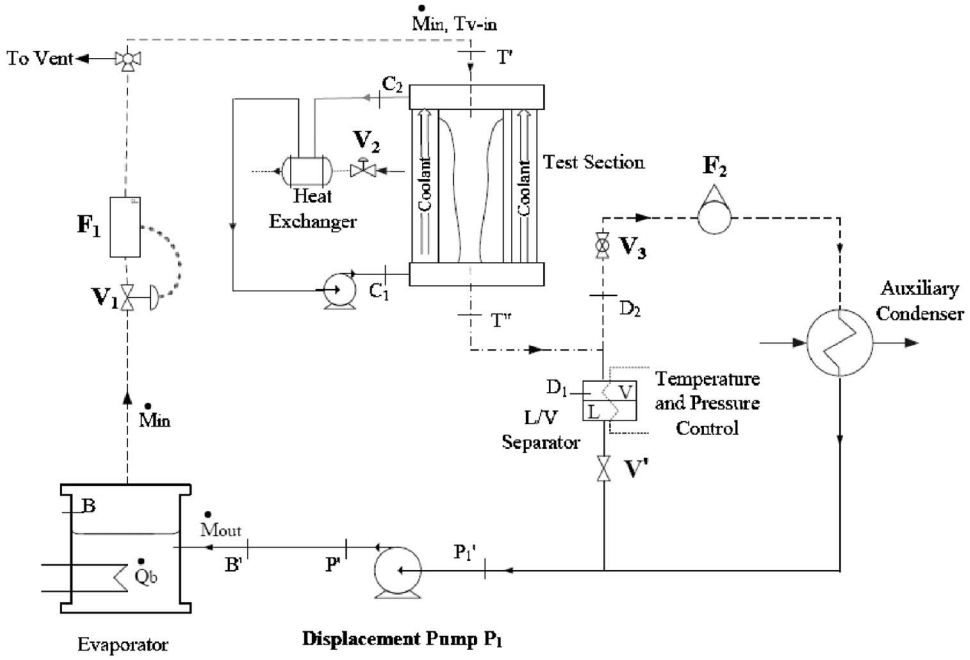

Fig. 4 The schematic of the flow loop for achieving unspecified exit-condition category II flows for partial or FC cases

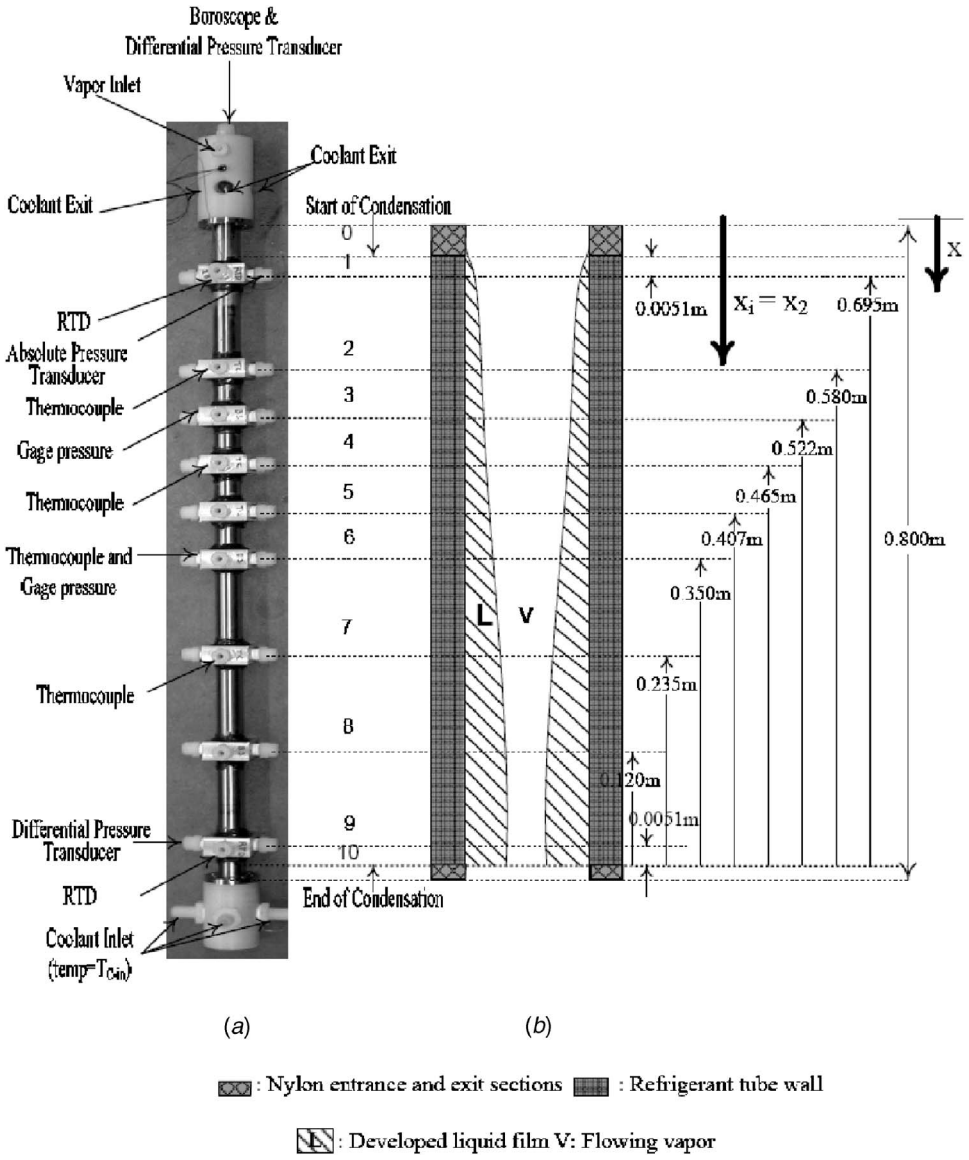

Fig. 5 (*a*) **The photograph of condenser test section.** (*b*) **The test-section schematic (diameters in** (*a*) **and** (*b*) **are not to the same scale). The condensing surface covers the zone** $x_0 \leqslant x \leqslant x_{10}$.

loop (see Kurita [33]) replaces the open drain water loop used in the preliminary experiments. This loop has two chillers in series (one for a coarse control and one for a finer control of temperature), and this provides for a good control of the steady value of temperature $T_{C\text{-in}}$ (marked in Fig. 5(*a*)) at the coolant inlet location in Figs. 3 and 4. This, in turn, enables the repetition of experimental runs regardless of seasonal variations in drain water temperature.

Resistance temperature detectors (RTDs) and type-T thermocouples measure temperatures at different locations of the test section (see Fig. 5) and at other flow loop locations marked by points B, B′, T′, C_1, C_2, D_1, D_2, P_1', P_2', and P′ in Figs. 3 and 4. A barometer measures outside atmospheric pressures. Flow meters at locations marked F_1 (Coriolis meter that directly measures mass flow rate), F_2 (a volume flow rate measuring rotameter), P_1 (volume flow rate meter imbedded in pump P_1), and P_2 (volume flow rate meter imbedded in pump P_2) yield mass flow rates through those locations. Absolute pressure transducers measure pressures at the test-section inlet (location 1 in Fig. 5) and at locations B and D_2 in Figs. 3 and 4. Differential pressure transducers measure pressure differences in the test section (in Fig. 5(*a*), this is between locations 1 and 9, location 3 and outside atmosphere, and location 6 and outside atmosphere). Two electronically controllable displacement pumps, P_1 and P_2 (see Figs. 3 and 4), can pump liquid FC-72 at a steady or unsteady specification of volume or mass flow rates. A pneumatically controlled valve V_1 is used, as needed, to control mass flow rate through F_1. Most of the details of the employed data acquisition system are explained in Narain et al. [31] and Siemonko [32].

For convenience, the system in Figs. 3 and 4 is broken into the following subsystems. (i) Subsystem A is the portion of the flow loop between points P′ and T′ (this portion contains the flow into the evaporator, the evaporator, the flow meter F_1, valve V_1, and the tubing leading the flow into the test section). (ii) Subsystem B is the portion of the flow loop between points T′ and T″ (this portion consists of the test section). (iii) Subsystem C is the portion of the flow loop between points T″ and P′ (this portion consists of the *L*/*V* separator, the two branches of the flow in the liquid line and the auxiliary-condenser line, and the pump or pumps). (iv) Subsystem D is the portion that consists of a primary

coolant loop (shown in Figs. 3 and 4 and a secondary coolant loop (not shown here but shown in Kurita [33]). The subsystems A–D defined above are not marked in Figs. 3 and 4, but the definitions introduced here are necessary for later discussions of the experimental results.

Additional details of this experimental facility (in fact, of a similar earlier version), data acquisition, and LABVIEW 7.1 based data processing and instrument control strategies are available in Siemonko [32].

3 Experimental Procedure

Here, we describe the procedure for investigating partial and FC cases under different exit conditions. Note that results from different exit conditions are to be compared for approximately the same inlet mass flow rate $\dot{M}_{\text{in}}$, inlet pressure p_{in}, and temperature difference $\overline{\Delta T}=T_{\text{sat}}(p_{\text{in}})-\bar{T}_w$, where $\bar{T}_w$ is the mean condensing surface temperature. Pure vapor may be allowed to enter the test section with a superheat of 2–10°C. The purging process (see Ref. [32]) ensures that the vapor flowing in the test section is pure over the duration of the experimental run and that noncondensable air in the flow loop has zero to insignificant presence. Note that vapor Jakob numbers $\text{Ja}|_V$ ($\equiv C_p|_V \Delta T_{\text{sup}}/h_{\text{fg}}(p_{\text{in}})$), where $C_p|_V$ is the specific heat of the vapor and $h_{\text{fg}}(p_{\text{in}})$ is the heat of vaporization at pressure p_{in}, represent the ratio of sensible cooling of vapor to heat of vaporization. Since these numbers are very small ($<1.0\times10^{-5}$) in comparison to liquid Jakob numbers Ja ($\equiv C_p|_L \cdot \overline{\Delta T}/h_{\text{fg}}(p_{\text{in}})$), where $C_p|_L$ is the specific heat of the liquid condensate), vapor temperature can be effectively modeled as a steady constant equal to the inlet saturation temperature. The steadiness of $\dot{M}_{\text{in}}$ primarily depends on the constancy of heat supply to the evaporator (which is easily achieved by constant electric heating at a known wattage) and the eventual approximate steadiness of the evaporator pressure p_b. Even if the steady value of p_b changes somewhat for different start-ups, as long as the corresponding evaporator saturation temperature T_b changes negligibly, it is found that the remaining flow loop pressures relative to a single effective boiler pressure are the same for two independent repetitions of the same experimental run (i.e., same $\dot{M}_{\text{in}}$, $\overline{\Delta T}$, $\bar{T}_w$, and Z_e). This is true because all other pressures p are effectively characterized by their pressure differences, $p-p_b$, relative to this pressure p_b. Alternatively, a previously obtained steady value of p_b can be regained by bringing the new evaporator pressure back to roughly this same value by suitably switching the heater on and off under the same steady heating rate or by gradually venting the evaporator from a higher pressure to the desired earlier value of p_b. Both of the above described processes have been used to successfully assess the repeatability of a few representative experimental runs. With regard to constancy of water temperature $T_{C\text{-in}}$ at the coolant inlet for the test section (see Fig. 5) over time, achieving constancy of water temperature and its flow rate in the secondary coolant loop (not shown here) proved to be sufficient.

3.1 Specified Exit Conditions (Category I Flows)

3.1.1 Incomplete or Partial Condensation Flows. For an investigation of partial condensation flows through the test section that involve specified conditions (through a steady and specified exit vapor quality) at the exit, the arrangement in Fig. 3 is used. In this arrangement, the liquid at the exit flows out of the test section at a mass rate of $\dot{M}_L$, goes through the liquid/vapor (L/V) separator, and is pumped by pump P_1 back into the evaporator. Both pumps P_1 and P_2 (displacement pumps made by Masterflex) in Fig. 3 allow a digital control of flow rates. The vapor at the exit flows out of the test section at a mass flow rate of $\dot{M}_V$ and is measured through a volume and mass flow rate measuring rotameter F_2. This vapor then flows through an auxiliary condenser where the vapor is completely condensed into liquid, goes through pump P_2, and then, on its way to the evaporator, merges near point P' (see Fig. 3) with the liquid flowing out of pump P_1.

The control strategy, to achieve a specified steady flow with a prescribed exit vapor quality ($\dot{M}_V/\dot{M}_{\text{in}} \equiv Z_e$) for a given inlet and wall conditions, is to initially hold valve V_1 open at a fixed level of opening while ensuring (as described in the first paragraph of this section) desired steady values of $\dot{M}_{\text{in}}$, p_b, and $\overline{\Delta T}$. Then, the exit vapor mass rate $\dot{M}_V$ through pump P_2 (or rotameter F_2) is held fixed at a value less than the inlet mass rate $\dot{M}_{\text{in}}$, while the exit liquid mass flow rate $\dot{M}_L$ is varied through pump P_1 at a value given by the tracking equation $\dot{M}_L|_{P_1}=\dot{M}_{\text{in}}-\dot{M}_V|_{\text{rotameter}}$.

As the flow through the evaporator becomes steady, $\dot{M}_{\text{in}}$ becomes steady, and, at that time, we may or may not need to hold this value actively fixed with the help of controllable valve V_1. At this stage, active control of valve V_1 does not achieve much, except that it eliminates some unwanted minuscule drifts in the inlet mass rates. For a given set of inlet ($\dot{M}_{\text{in}}, p_{\text{in}}, T_{V\text{-in}}$) and wall ($\bar{T}_w$) conditions, different specified steady states are achieved by the above strategy for different values of $\dot{M}_L$. Experimentally achieved examples of specified exit category I partial condensation flows are discussed in the next section.

3.1.2 Complete or Full Condensation Flows. The experimental technique for prescribing different exit pressures in FC cases is important but has not yet been implemented. Typically, one would need to specify different pressures at the exit of the test section, at the L/V separator (see Figs. 3 and 4), which is downstream of the "point of FC." This requires active pressure control at the L/V separator. Fully condensing category I flows achieved in this fashion do, however, become equivalent to category III flows with fixed valve settings (k_i and k_e) introduced in the definition of category III flows. This is part of an ongoing research. Therefore, results for this important case are not reported here.

3.2 Unspecified Exit-Condition Cases (Category II Flows)

3.2.1 Natural Partial Condensation. For obtaining/investigating the existence of a "long-term" and steady natural exit condition for category II flows (under unspecified exit conditions) with all other conditions being kept the same as in a corresponding specified exit-condition case in category I, the flow is required to go through the test section and onwards under the arrangement shown in Fig. 4. Note that this arrangement has a single displacement pump as opposed to the two displacement pumps used in the arrangement of Fig. 3. The approach is to hold values of $\dot{M}_{\text{in}}$, p_b, and $\overline{\Delta T}$ nearly the same as in one of the specified category I cases while the pump P_1 in Fig. 4 is *controlled* such that the mass flow rate through it tracks the equation: $\dot{M}_L|_{P_1}=\dot{M}_{\text{in}}$. If the start-up and other conditions allow, a steady state flow is attained in which, by the exit, the inlet vapor mass flow rate is split, by a natural selection process, into a liquid condensate flow rate $\dot{M}_L|_{\text{Na}}$ and a vapor flow rate $\dot{M}_V|_{\text{Na}}$. Clearly, these values satisfy the equation $\dot{M}_{\text{in}}=\dot{M}_L|_{\text{Na}}+\dot{M}_V|_{\text{Na}}$. Experimentally achieved examples of unspecified exit category II partial condensation flows are discussed in the next section.

3.2.2 Complete or Full Condensation Flows With a Natural Steady State. For achieving FC flows in the test section, valve V_3 in Fig. 3 is shut and the arrangement in Fig. 3 is then used. Here, we choose the controlling temperature difference $\overline{\Delta T}=T_{\text{sat}}(p)-\bar{T}_w$ to become sufficiently large for a fixed inlet mass flow rate to ensure that one achieves, through the indicated procedures for the setup, a steady flow in Fig. 3 with a natural $\dot{M}_V=0$ (an approximate value obtained even if V_3 was to be left open).

Table 1 Experimentally measured data and some key calculated and computed variables for steady states achieved for category II (unspecified exit-condition) partial condensation flows

Run No	$\dot{M}_{in}$ (g/s)	$\dot{M}_V$ (g/s)	Z_e exp	Z_e comp	$\bar{T}_W$ (K)	T_{sat} (K)	$\overline{\Delta T}$ (K)	p_{in} (kPa)	p_{x6} (kPa)	$p_{T''}$ (kPa)	Δp (kPa)	p_{D2} (kPa)	ρ_2/ρ_1	μ_2/μ_2	G (kg/m^2 s)	Re	Ja	Pr_1	$\dot{Q}_{out}$ (J/s)	$\bar{q}'$ (W/m^2)	$\bar{h}$ (W/m^2 K)
No	±0.05	±0.04	±0.04		±1	±0.15	±1	±0.6	±0.6	±0.7	±0.05	±2	±0.0001	±0.0001	±1.5	±900	±0.02	±0.02	±5	±800	±80
1	1.44	0.48	0.33	0.33	320	331.49	11	107.3	109.3	106.5	–0.82	105	0.0085	0.0243	42.1	23,900	0.14	9.61	81	5200	453
2	1.76	1.08	0.62	0.57	317	325.23	8	87.0	86.4	88.0	–0.36	85	0.0070	0.0223	51.5	29,700	0.10	10.11	58	3700	450
3	1.54	0.69	0.44	0.36	323	335.55	12	122.6	116.6	116.1	–0.19	114	0.0097	0.0260	45.0	25,300	0.15	9.21	71	4500	387
4	1.29	0.49	0.38	0.38	320	329.64	10	101.0	102.4	100.8	–2.09	98	0.0081	0.0230	37.7	21,500	0.11	9.69	68	4300	476
5	1.70	0.83	0.51	0.52	324	332.55	9	111.0	112.5	111.0	–0.93	109	0.0089	0.0252	49.6	28,100	0.11	9.37	70	4400	508
6	1.17	0.47	0.40	0.39	320	332.64	13	111.3	NA[b]	111.3	–0.12	109	0.0088	0.0246	34.2	19,325	0.16	9.55	59	3700	298
7	1.31	0.49	0.37	0.37	321	330.85	10	105.0	106.8	104.5	–2.06	102	0.0084	0.0244	38.3	21,700	0.12	9.58	69	4400	462
8[a]	1.93	1.39	0.72	0.72	322	325.55	4	84.6	NA[b]	NA[b]	0.01	NA[b]	0.0071	0.0231	56.4	32,500	0.05	9.85	47	3000	742
9	1.59	1.11	0.69	0.63	328	334.25	6	113.0	NA[b]	NA[b]	NA[b]	NA[b]	0.0094	0.0265	46.5	26,200	0.08	9.07	40	2500	418
10	2.12	1.37	0.64	0.64	320	327.85	8	91.4	NA[b]	NA[b]	–0.10	NA[b]	0.0076	0.0234	62.0	35,500	0.10	9.83	64	4100	503
11	1.30	0.45	0.35	0.38	321	329.29	8	99.8	100.2	99.7	–1.62	97	0.0080	0.0240	38.0	21,700	0.10	9.70	72	4600	537

[a]The error values for this case were greater than the representative error values shown in the column headers due to small $\overline{\Delta T}$ and high relative error associated with its measurement.
[b]NA: The data were not available due to some equipment problem.

For the natural FC case, the valve V_1 in Fig. 3 is left open at a fixed opening and pump P_1 is controlled to always satisfy, in time, the relation $\dot{M}_L|_{P_1} = \dot{M}_{in}$. If a steady state is achieved, this leads to a natural steady FC flow (i.e., as will be discussed later, if $X_{FC} < L$ in Fig. 9). The word natural is also used here because the use of displacement pump P_1 in the arrangement downstream of the test section allows the test-section vapor flow to attain whatever pressure it desires by the test-section exit or by the point of FC. Because of experimental limitations in measuring X_{FC}, at present, $X_{FC} < L$ is assured only through a computational simulation. Also, note that because of the unspecified (free) exit condition, this way of achieving steady FC flows is expected to keep vapor density nearly uniform.

4 Experimental Results, Discussions, and Comparisons with Simulations

The column headers in Tables 1–3 indicate accuracies of the values of key *measured* variables obtained through flow loop instruments and sensors. Overall accuracy bounds for the reported calculated variables (such as $\bar{q}''$, $\bar{h}$, etc.) are also shown. The nondimensional numbers Re_{in}, $x_e = L/D = 106$, Ja, ρ_2/ρ_1, and μ_2/μ_1 in Tables 1–3 define the flows, and they are defined in Refs. [1–3]. In Tables 1–3, the heat flow rate $\dot{Q}_{out}$ and associated average heat-transfer coefficients ($\bar{h}$) are obtained through the relation $\dot{Q}_{out} \approx \dot{M}_L h_{fg} = \bar{h}(\pi DL)\overline{\Delta T}$. The inlet vapor mass flux G in Tables 1–3 is defined as $4\dot{M}_{in}/(\pi D^2)$.

All (except the Coriolis meter F_1) of the instruments' accuracies for measured variables were established after their in-house calibrations with the help of suitable and reliable reference instruments of known resolution and appropriate reference physical conditions (temperature, flow rate, pressure, etc.). The accuracy of the Coriolis meter was established by the vendor support staff at the time of its installation. The error estimates for the calculated variables reported in Tables 1–3 were obtained by well-known standard procedures (see, e.g., Eqs. (3.27) and (3.28) in Ref. [34]). The accuracies of individual calculated variables in a column were taken into account to report maximum values of the errors in the column headers of Tables 1–3. All the individual values of errors were either less than or equal to these reported error values. The error definitions, associated error analyses, and calibration accuracies can be found in Narain et al. [31].

The experimental runs reported in the next section were taken after ensuring that (i) representative runs were repeatable, (ii) the mass flow rates for partial condensation cases added up to satisfy the mass balance, (iii) the overall energy balance for the test section was satisfied, i.e., $\dot{M}_{in} h_{fg} \approx \dot{M}_w C_{pw} \cdot \Delta T_w$, where for a representative FC case, ΔT_w is the rise in the water temperature in the annulus surrounding the test-section, and (iv) various data were reasonable (based on simulation estimates) and consistent with one another. The experimentally obtained partial condensation cases in category II (unspecified exit) are listed in Table 1 with all the essential details, including exit vapor quality Z_e (fourth column) and its value obtained from simulations (fifth column). The corresponding partial condensation flow cases under category I (specified exit-condition cases) are listed in Table 2. The experimental data for category II FC cases are reported in Table 3. The values for pressure drop across the test section were found to be negative for almost all of the cases that have been reported here, indicating that pressure at the exit was greater than that at the inlet. This is because of the typical range of $\dot{M}_{in}$ and $\overline{\Delta T}$ we have been operating in (0.5–2 g/s and 2–12°C, respectively). Further, the magnitude of experimental pressure rise was found to be higher than predictions obtained from the laminar-vapor/laminar-condensate simulation tool employed in this paper. The results and discussions for exit-condition categories I and II are described below, separately, for partial and FC flows.

Table 2 Experimentally measured data and some key calculated variables for steady states achieved for category I (specified exit-condition) partial condensation flows

Run No	M_{in} (g/s) ±0.05	M_V (g/s) ±0.04	Z_e exp ±0.04	$\bar{T}_W$ (K) ±1	T_{sat} (K) ±0.15	$\overline{\Delta T}$ (K) ±1	p_{in} (kPa) ±0.6	p_{x6} (kPa) ±0.6	$p_{T''}$ (kPa) ±0.7	Δp (kPa) ±0.05	p_{D2} (kPa) ±2	ρ_2/ρ_1 ±0.0001	μ_2/μ_2 ±0.0001	G (kg/m^2 s) ±1.5	Re ±900	Ja ±0.02	Pr_1 ±0.02	$\dot{Q}_{out}$ (J/s) ±5	$\bar{p}'$ (W/m^2) ±800	$\bar{h}$ (W/m^2 K) ±80
1	1.44	0.52	0.36	320	331.91	12	108.8	110.9	108.0	−1.82	106	0.0087	0.0244	42.1	23,800	0.15	9.59	78	4900	416
2	1.31	0.50	0.38	320	329.16	9	99.4	100.3	99.5	−0.43	98	0.0080	0.0238	38.4	21,900	0.11	9.72	69	4400	505
3	1.34	0.59	0.44	320	328.55	9	97.4	98.4	97.3	−0.32	96	0.0078	0.0236	39.1	22,400	0.10	9.76	64	4100	491
4[a]	1.80	0.64	0.36	323	330.53	8	103.9	105.9	104.4	−0.59	103	0.0083	0.0246	52.6	29,900	0.09	9.50	97	6200	851
5[a]	1.92	1.00	0.52	323	329.64	7	101.0	103.3	101.7	−0.40	100	0.0081	0.0244	56.1	32,000	0.08	9.55	78	4900	771
6	1.20	0.00	0.00	320	332.23	12	110.5	113.2	110.5	−0.80	108	0.0088	0.0245	35.0	19,800	0.16	9.57	101	6400	514
7	1.22	0.44	0.35	320	331.71	12	108.0	110.6	108.0	−0.62	106	0.0086	0.0243	36.6	20,200	0.15	9.62	66	4200	351
8[a]	1.93	1.15	0.60	322	325.21	3	87.15	NA[b]	NA[b]	−1.30	NA[b]	0.0071	0.0231	56.4	32,600	0.04	9.87	67	4300	1174
9	1.61	1.14	0.70	322	332.57	11	111.4	104.6	107.0	−0.87	103	0.0089	0.0250	47.1	26,630	0.13	9.46	35	2200	212
10	1.67	1.37	0.82	322	331.45	10	105.8	98.6	100.8	−0.74	97	0.0085	0.0245	49.0	27,800	0.12	9.57	16	1000	108
11	1.81	1.02	0.56	317	331.48	14	106.8	102.1	NA[b]	−0.58	99	0.0085	0.0237	52.9	30,000	0.18	9.80	54	3400	236
12	1.66	0.60	0.36	318	333.15	15	113.5	108.6	NA[b]	−1.46	106	0.0090	0.0243	48.5	27,400	0.20	9.66	88	5600	363
13	1.71	0.49	0.28	316	331.14	15	108.0	107.9	108.1	−2.10	105	0.0085	0.0237	50.1	28,400	0.19	9.81	103	6500	441
14	1.30	0.65	0.50	320	326.34	6	90.5	92.1	90.5	−1.15	88	0.0073	0.0230	38.0	21,800	0.08	9.90	56	3500	545
15	1.29	0.55	0.43	321	331.63	11	107.7	113.2	110.1	−1.60	107	0.0086	0.0245	37.7	21,400	0.14	9.57	62	3900	366
16	1.31	0.76	0.58	321	331.07	11	105.8	109.1	105.8	−0.95	104	0.0084	0.0243	38.3	21,700	0.13	9.62	46	2900	279
17	1.14	0.88	0.77	319	326.73	8	91.6	92.8	91.9	−0.14	90.4	0.0074	0.0230	33.5	19,300	0.09	9.92	22	1400	186
18	1.39	0.64	0.46	318	329.01	11	98.9	101.3	98.4	−0.65	97.1	0.0079	0.0234	40.6	23,200	0.14	9.85	64	4100	377

[a]The error values for this case were greater than the representative error values shown in the column headers due to $\overline{\Delta T}$ and high relative error associated with its measurement.
[b]NA: The data were not available due to some equipment problem.

Table 3 Experimentally measured data and some key calculated variables for steady states achieved for category II (unspecified exit-condition) FC flows

Run No	M_{in} (g/s) ±0.05	$\bar{T}_W$ (K) ±1	T_{sat} (K) ±0.15	$\overline{\Delta T}$ (K) ±1	p_{in} (kPa) ±0.6	p_{x6} (kPa) ±0.6	$p_{T''}$ (kPa) ±0.7	Δp (kPa) ±0.05	p_{D2} (kPa) ±2	ρ_2/ρ_1 ±0.0001	μ_2/μ_1 ±0.0001	G (kg/m^2 s) ±1.5	Re ±800	Ja ±0.02	Pr_1 ±0.02	$\dot{Q}_{out}$ (J/s) ±5	$\bar{q}''$ (W/m^2) ±500	$\bar{h}$ (W/m^2 K) ±26
1	0.69	304	326.93	23	92.3	94.9	90.8	−1.13	89	0.0073	0.0207	20.2	11,600	0.28	10.74	59	3800	165
2	0.70	304	328.46	24	97.2	99.8	95.5	−1.54	94	0.0077	0.0210	20.4	11,700	0.30	10.65	60	3800	156
3	1.01	317	329.67	13	101.1	104.0	100.1	−0.57	99	0.0081	0.0234	29.7	17,000	0.16	9.87	86	5500	438
4	0.86	316	330.20	14	102.8	104.1	101.4	−3.05	99	0.0082	0.0234	25.1	14,300	0.17	9.88	73	4600	331
5	0.96	304	326.95	23	92.4	93.1	90.4	−0.62	89	0.0074	0.0208	28.1	16,000	0.28	10.72	82	5200	230
6	0.75	302	328.61	27	97.6	98.2	95.4	−3.01	92	0.0077	0.0207	22.0	12,500	0.33	10.79	64	4000	151
7	0.62	302	327.17	25	93.0	94.8	91.1	−2.41	89	0.0074	0.0204	18.1	10,400	0.31	10.86	53	3375	133
8	0.63	301	326.97	26	92.4	94.2	90.5	−0.54	90	0.0073	0.0203	18.4	10,600	0.39	10.90	54	3400	134
9	0.48	301	327.07	26	92.8	94.6	90.7	−1.18	90	0.0074	0.0209	14.0	8000	0.32	10.90	41	2600	102
10	0.78	305	341.13	36	146.0	NA[a]	NA[a]	−0.35	129	0.0116	0.0240	22.9	12,700	0.47	9.95	64	4100	112
11	0.97	316	343.27	27	155.8	NA[a]	NA[a]	−0.33	140	0.0127	0.0265	28.3	15,600	0.37	9.25	79	5000	180
12	0.87	300	343.11	43	155.0	NA[a]	NA[a]	−0.14	138	0.0125	0.0236	25.4	14,000	0.57	10.06	71	4500	104
13	0.80	306	342.02	36	150.0	NA[a]	NA[a]	−0.25	136	0.0120	0.0244	23.4	12,900	0.48	9.80	65	4200	115
14	0.80	322	340.69	19	144.1	135.7	140.4	−0.29	143	0.0115	0.0277	23.6	13,000	0.25	9.04	66	4200	228
15	0.99	324	342.32	18	151.4	NA[a]	152.3	−2.05	148	0.0123	0.0279	29.2	16,000	0.24	8.87	81	5200	283
16	1.59	306	333.56	27	115.0	110.5	109.3	−0.24	112	0.0090	0.0225	46.4	26,100	0.35	10.25	133	8400	309
17	0.76	324	337.82	14	131.7	125.7	126.3	−0.23	130	0.0105	0.0266	22.2	12,400	0.18	9.10	63	4000	289
18	1.30	312	331.98	19	109.4	111.4	108.5	−1.32	107	0.0087	0.0231	38	21,500	0.25	10.00	109	6900	350

[a]NA: The data were not available due to some equipment problem.

4.1 Partial Condensation Flows

4.1.1 Specified Exit-Condition (Category I) and Unspecified Exit-Condition (Category II) Cases. For partial condensation, Fig. 6(*a*) shows the attainment of two specified exit-condition case steady/quasisteady flows marked Specified-1 ($t_2 \leqslant t(\text{min}) \leqslant t_2+20$) and Specified-2 ($t_3 \leqslant t(\text{min}) \leqslant t_3+30$). The Specified-1 and Specified-2 cases correspond to run 1 and run 18, respectively, in Table 2. The results over time interval $t_4 \leqslant t(\text{min}) \leqslant t_4+20$ show the experiment's ability to approximately repeat the data for a case that is approximately the same as Specified-1 and is termed as Specified-1 Approx. Following the method described in Sec. 3, Figs. 6(*a*) and 6(*b*) also show, over the time interval $t_1 \leqslant t(\text{min}) \leqslant t_1+76$, the attainment of a corresponding natural steady exit condition and associated steady flow variables for an unspecified exit-condition (category II) case. This case corresponds to run 1 in Table 1. The Natural-1, Specified-1, and Specified-2 steady states (in Figs. 6(*a*)–6(*c*)) have the same values of $\dot{M}_{\text{in}} \approx 1.40 \pm 0.05$ g/s and $\overline{\Delta T} \approx 11 \pm 1\,^{\circ}\text{C}$ but different values of $\dot{M}_L$ and $\dot{M}_V$ that satisfy $\dot{M}_L|_1 + \dot{M}_V|_1 = \dot{M}_L|_2 + \dot{M}_V|_2 = \dot{M}_{\text{in}}$. The differences between the Specified-1 and Specified-2 cases are as follows: (i) they have different heat-transfer rates (since energy balance gives $\dot{Q}_{\text{out}} \approx \dot{M}_L h_{\text{fg}}$). The two cases have approximate heat-transfer rates of 78 ± 4 W and 64 ± 4 W and average heat-transfer coefficients of 416 ± 40 W/m^2 K and 377 ± 40 W/m^2 K, respectively. (ii) The two cases also have different hydrodynamics, the signature of which is clear through corresponding computational simulations and through the difference between experimentally obtained mean values of Δp for the two cases (in Table 2 they are -1.82 kPa and -0.65 kPa, respectively). Furthermore, specified (category I) and unspecified (category II) flows have different dynamic responses to a disturbance (in Figs. 6(*a*)–6(*c*), a disturbance was induced by momentarily shutting or decreasing the opening in the valve V_1 shown in Figs. 3 and 4). The difference in dynamic response is seen by comparing Specified-2 and Natural-1 cases for the transient decay time τ_D associated with the exit vapor flow rate $\dot{M}_V$ in Fig. 6(*a*) or τ_D associated with Δp in Fig. 6(*b*). In Fig. 6(*a*), the rapid shutting or closing of valve V_1 caused the indicated responses in the $\dot{M}_{\text{in}}$ time history. For the Natural-1 case, this response is as shown in Fig. 6(*a*), but a more rapid response for the Specified-2 case is not captured by the resolution of the figure and it is indicated by a dotted line. With regard to dynamic responses to a disturbance, it is clear that the Specified-2 case of Fig. 6(*a*) (though it is farther from a natural case) is more stable than the Natural-1 case because its transient decay time τ_D is much shorter. In other words, natural steady states for unspecified exit conditions (category II) are generally more noise sensitive because the exit in category II cases is not as isolated from flow variation further downstream of it, as is the exit for specified exit-condition cases (category I), and this causes an additional lingering impact of noise arising from the flow variables in the exit zone. Time histories of pressure and temperature values in subsystems A, C, and D for the cases in Figs. 6(*a*)–6(*c*) are not shown here for brevity but are available in Figs. 7(d)–7(e) of Narain et al. [31].

The cases shown in Figs. 6(*a*)–6(*c*) are representative runs taken from a set of partial condensation runs for specified (category I) and unspecified (category II) exit-condition cases in Tables 1 and 2. The data matrix associated with these partial condensation category I and category II cases is best represented by Fig. 7. The test matrix for all partial condensation (including both categories I and II) cases is limited by the system limits and flow regime boundaries indicated on the plane marked by inlet mass flow rate $\dot{M}_{\text{in}}$ and temperature difference $\overline{\Delta T}$ values. Figure 7 shows all the partial condensation cases plotted on the two dimensional plane formed by $\dot{M}_{\text{in}}$ and $\overline{\Delta T}$. These parameters were found to be the key variables controlling the dynamics of the condensing flows in the test section. The typical values for lower and upper limits for the inlet mass flow rate were found to be 1 g/s and 2 g/s, respectively, and those for the $\overline{\Delta T}$ were recorded to be 2 °C and 12 °C, respectively. The interior shaded zone in Fig. 7 represent $\dot{M}_{\text{in}}$ and $\overline{\Delta T}$ values, for which steady flows were attained for both specified (category I) and unspecified (category II) exit-condition cases. The bounding curve B in Fig. 7 indicates a lower threshold of $\overline{\Delta T}$ such that steady condensing flows attained below that curve (see points marked in Fig. 7) were dropwise patchy—i.e., not annular—on the condensing surface near the inlet. Below this curve, the condensation, as observed from the inlet boroscope, indicates that the flow is no more film annular near the point of onset of condensation as there are wet and dry patches associated with dropwise condensation. This happens because the $\overline{\Delta T}$ value is below a lower threshold. The bounding curve B is partly experimental, and curve C on the right in Fig. 7 is, at present, entirely schematic (i.e., not fully explored by experiments). Curve C represents an expected transition to wispy-annular flows (see Fig. 10.3 in Carey [35]) at very high $\dot{M}_{\text{in}}$ at any $\overline{\Delta T}$. The dotted curve A on the left bottom has been experimentally noticed. It does not represent a flow regime boundary for the test section, as it is a result of the exit pressure oscillations or unsteadiness in the test section imposed by oscillatory or other plug/slug instabilities occurring elsewhere in the system (in this case, in the auxiliary condenser downstream of the test section). An example of such an instability case is discussed in Sec. 5. The bounding curve in the upper left corner of Fig. 7 is marked as curve D. This curve represents a transition from partial condensation to FC. If $\dot{M}_{\text{in}}$ is reduced and $\overline{\Delta T}$ is increased further, computations show that the left side of curve D represents the zone for which the entire vapor coming in condenses inside the test section (i.e., for category II flows, X_{FC} in Fig. 9 starts satisfying $X_{\text{FC}} \leqslant L$ on the left side of curve D as opposed to $X_{\text{FC}} > L$ on the right side of curve D). Note that Fig. 9 suggests, in accord with computations as well as remarks of Rabas and Arman [8], that this point of FC does not necessarily imply an all liquid phase for $x > X_{\text{FC}}$. It simply means that the zone $x > X_{\text{FC}}$ is such that the average vapor mass flow rate $\dot{M}_V$ is zero and so are the interfacial mass and heat-transfer rates at these locations. Since the area on the left side of curve D represents FC, it is discussed in Sec. 4.1.2.

For a few data points in Fig. 7, the rotameter F_2 data were corrupted by the float's occasional stickiness to the rotameter walls. These cases are marked by unfilled circles in Fig. 7, and all the rest of the good cases (also based on comparisons with computational simulations) are marked by dark filled circles. These dark filled circles representing good partial condensation cases in Fig. 7 are actually the projections on the $\dot{M}_{\text{in}}$-$\overline{\Delta T}$ plane of the points reported in the three dimensional data matrix, which has $\dot{M}_{\text{in}}$, $\overline{\Delta T}$, and Z_e ($\equiv \dot{M}_V/\dot{M}_{\text{in}}$) as the three axes. This three-dimensional data matrix is not shown here for brevity but is shown in Fig. 8(b) of Narain et al. [31], where the figure is able to depict all the cases of category II (unspecified exit) as well as category I (specified exit) partial condensing flows. Each point in Fig. 7 represents, for given values of $\dot{M}_{\text{in}}$ and $\overline{\Delta T}$, a set of data consisting both category I cases and its associated unique natural category II case. There are, however, as seen in Fig. 8(b) of Narain et al. [31], some data sets representing only category I or category II cases. For each data set in Fig. 7 consisting of category I cases and the associated category II case, category I flows were found to be more robust and stable as compared to their associated category II counterparts.

4.1.2 Comparisons With Relevant Computational Results (Partial Condensation). Figure 8 shows the computationally obtained (employing the tools reported in Ref. [3]) steady and noise-free details of local film thickness and heat-flux variations for the specified and unspecified natural cases marked as Specified-2 (run

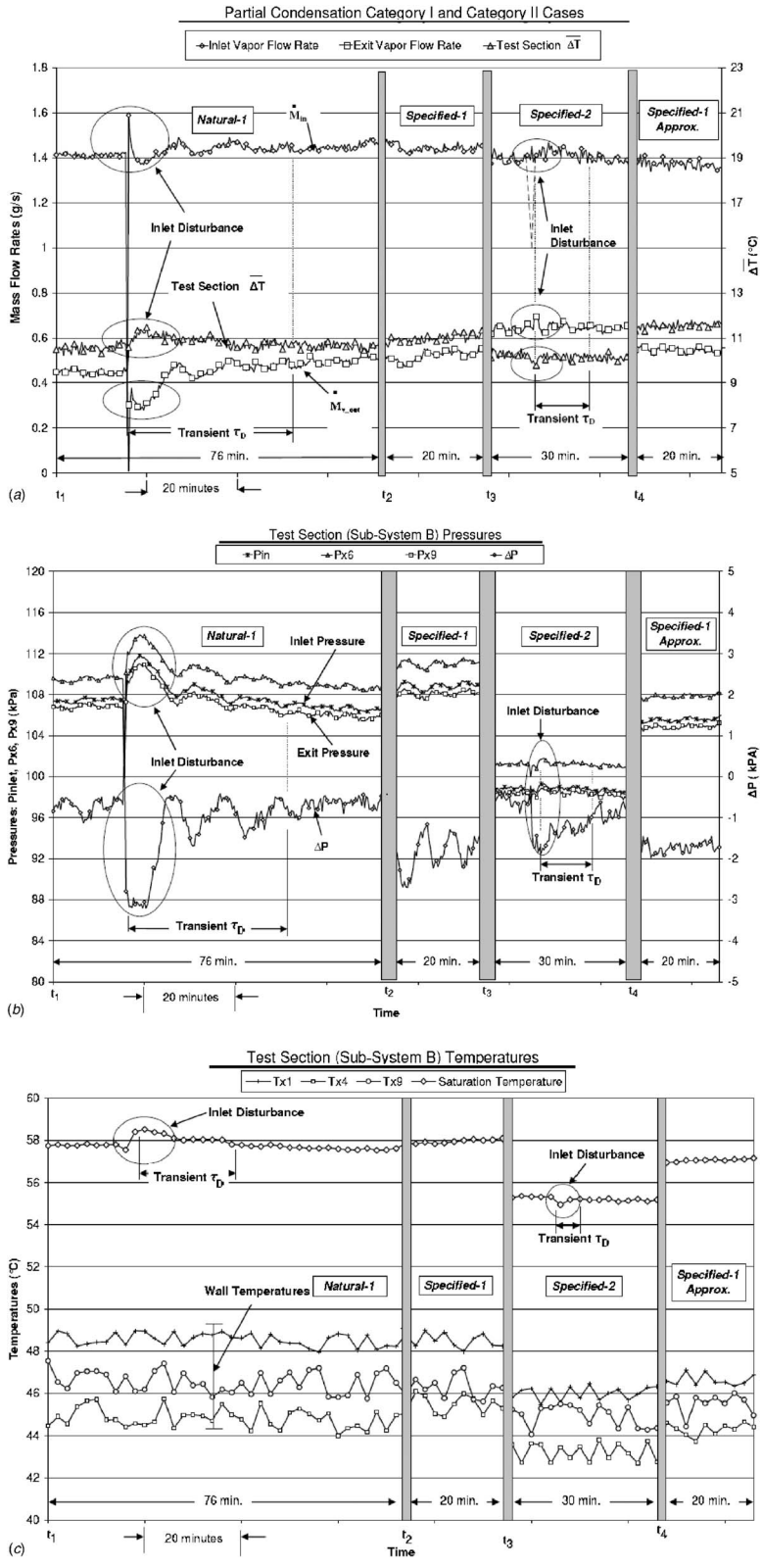

Fig. 6 (*a*) Time history depiction of $\dot{M}_{in}$, $\dot{M}_V$, and $\overline{\Delta T}$ values for multiple steady states of partial condensation cases, viz., Natural-1 (run 1 from Table 1), Specified-1 (run 1 from Table 2), Specified-2 (run 18 from Table 2), and Specified-1 Approx. (*b*). Time history of pressures (along the test section) and Δp values (across the test section) for the cases shown in (*a*) (*c*) Time history of temperature values along the test section (subsystem B) and T_{sat} (p_{in}) for the cases shown in (*a*).

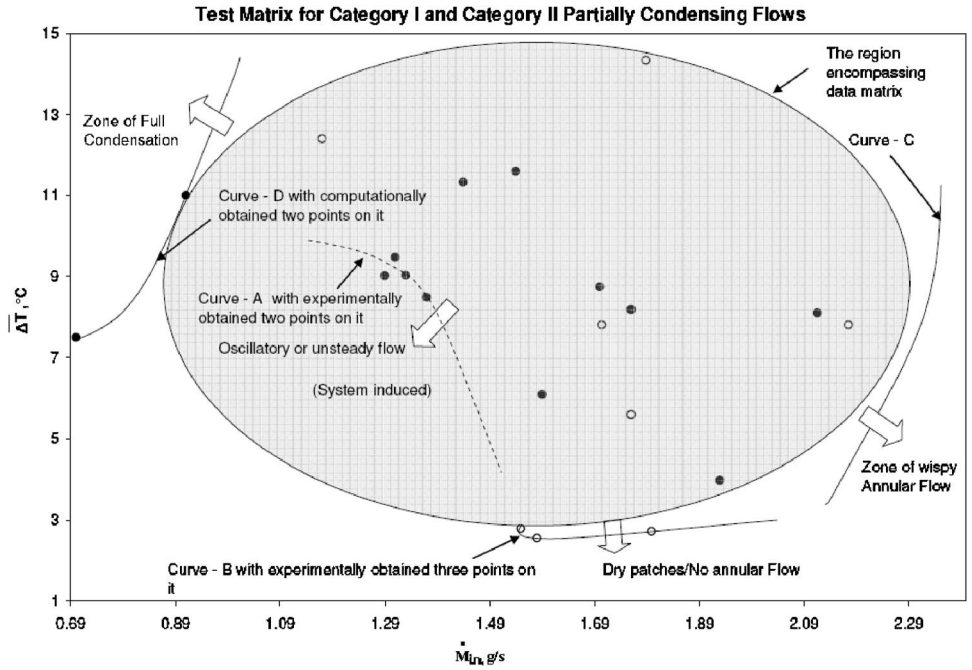

Fig. 7 Two-dimensional test data matrix for category II (unspecified exit condition) partial condensation flow cases and different bounding curves represented on the $\dot{M}_{in}-\overline{\Delta T}$ plane

18 in Table 2) and Natural-1 (run 1 in Table 1) in Figs. 6(*a*)–6(*c*). The variation of vapor quality Z ($\equiv \dot{M}_v/\dot{M}_{in}$ at any x) along the test section can be easily obtained from the graphical results in Fig. 8 from the relation $Z(x) \equiv 1-[(\pi \cdot D)/(\dot{M}_{in} h_{fg})]\int_0^x q''_w dx$.

The exit vapor quality for the Specified-2 case was greater than that of the associated Natural-1 case. As a result, a higher amount of vapor condenses for the Natural-1 case, and this makes the heat-transfer rate $\dot{Q}_{out}$ for the natural case to be on the higher side (see Tables 1 and 2 for details). For all other conditions remaining the same, as observed from the computational results in Fig. 8, this makes the Natural-1 case's liquid film thickness lower and the wall heat flux higher than the values for the Specified-2 case. Such details of representative local variations in film thickness and heat flux are very important and should be more extensively synthesized with experimental results before heat-transfer correlations are developed for suitable categories and subcategories of internal condensing flows. However, reliable experimental information on local spatial variations of these quantities is not expected until later incorporation of film thickness sensors and heat-flux sensors in these experiments. Observe that the computationally obtained prediction of the natural exit vapor quality $Z_e|_{\text{Na comp}}$ ($\approx$0.33) for category II flow in Fig. 6(*a*)–6(*c*) is in a very good agreement with the experimentally obtained $Z_e|_{\text{Na Expt}}$ ($\approx$0.33) value (see Table 1). In fact, a very good agreement between $Z_e|_{\text{Na comp}}$ and $Z_e|_{\text{Na expt}}$ values was found for all category II cases in Fig. 7, and this is clear from their numerical values in Table 1. Note that a good agreement between experimental and theoretical Z_e values has also been obtained and reported (see Ref. [2]) for a shear driven condensing flow in a channel (category II experiments of Lu and Suryanarayana [27]).

The values of pressure drop Δp (p_{in}-p_{exit}) obtained from simulations for all the category II partial cases were negative and below 50 Pa, indicating that p_{exit} was greater than p_{in} for all the condensation cases in the given $\dot{M}_{in}$ range. This is confirmed by the experimental values of Δp (see Tables 1–3), which are also all negative (except for a very few cases). However, as expected, the magnitudes for experimental values of Δp were found to be greater than those from simulations. The reason behind this is that the simulations assume laminar-vapor/laminar-liquid flows while, in reality, the vapor Reynolds numbers are in the higher range (20,000–30,000), and this makes vapor flows significantly turbulent in the core (see Tables 1–3). The turbulence in the vapor core does not affect the mass transfer across the interface much because the condensate motion is gravity dominated. However, the turbulent vapor core significantly increases Δp values in the vapor domain. Because of this, the values of vapor quality obtained from the simulation are in good agreement with the experiments, but the values of pressure drop Δp obtained from experiments are higher in magnitudes. The predicted pressure drop Δp values do become comparable to experimental values if suitable corrections for vapor turbulence are made. The modifications in the computational procedure needed to account for vapor turbulence are explained in Narain et al. [31].

4.2 Complete or Full Condensation Flows

4.2.1 Specified Exit-Condition Cases (Category I Flows). As mentioned earlier, this case has not been investigated experimentally because the current setup does not have active pressure control strategies for fixing different pressures at the L/V separator, leading to different pressures at the inlet to pump P_1 (point P'_1 in Figs. 3 and 4). However, current computational simulations show that the location of the point of FC shown in the schematic of Fig. 9, is extremely sensitive to exit pressure p_e. For the gravity driven condensate in relatively large diameter tubes, the zone between the point of FC and the point of test-section exit is typically not filled with liquid alone (see the liquid marked by the doubly shaded zone in Fig. 9). Instead, this zone experiences a more complex two-phase flow with nearly zero interfacial mass or heat-transfer rates and nearly *zero average* vapor velocity or average vapor mass flow rate.

4.2.2 Unspecified Exit Condition Cases (Category II Flows). The test matrix (Table 3) for the natural steady FC cases under category II accommodates a range of vapor mass flow rates and temperature difference $\overline{\Delta T}$ values that are shown in Fig. 10. The shaded region in Fig. 10 contains most of the data points obtained for steady FC cases. More details on these cases are given in Table

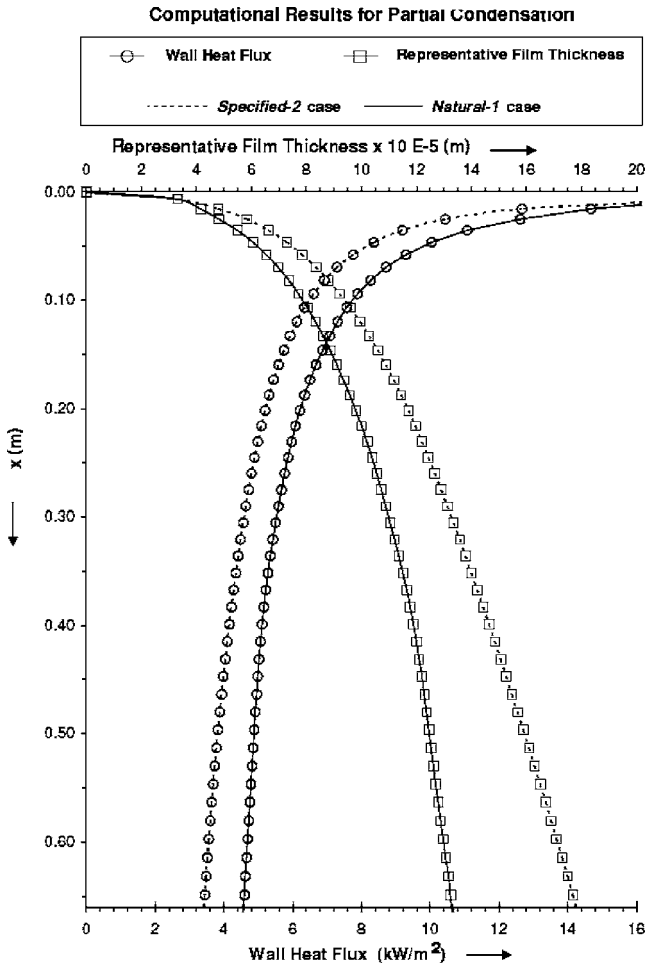

Fig. 8 For the Natural-1 and Specified-2 flow cases in Figs. 6(*a*)–6(*c*), this figure shows the computationally obtained representative film thickness and wall heat-flux variation along the test section. The film thickness and heat-flux values shown have been obtained for smooth interface conditions. In reality, they are modulated by waves due to presence of noise (see Ref. [3]).

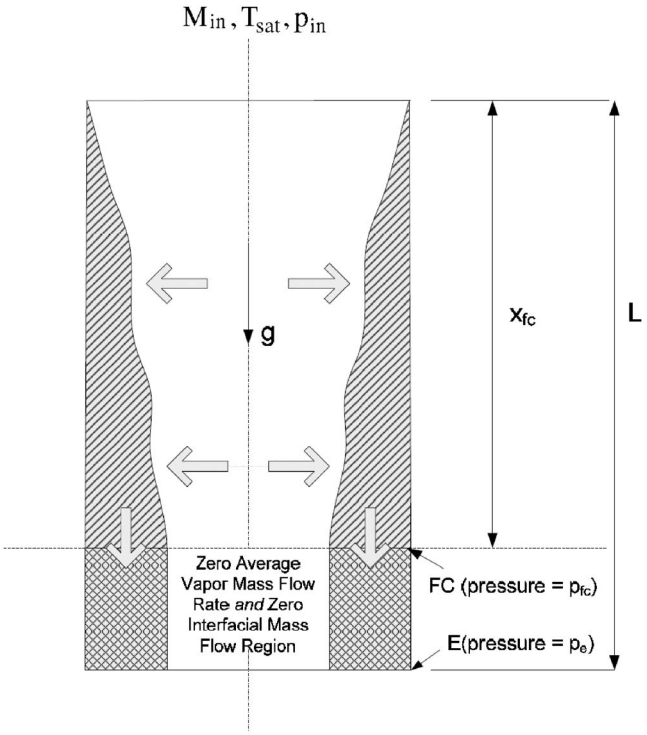

Fig. 9 The schematic of FC showing point of FC and its downstream region with zero interfacial mass and heat transfer.

3 along with the accuracies of measured and calculated variables. For representative FC cases in Table 3, Figs. 11(*a*)–11(*c*) show three steady states: Natural-1 over $t_1 \leq t(\text{min}) \leq t_1+30$ (Table 3, run 1 with $\dot{M}_{\text{in}} \approx 0.69 \pm 0.05$ g/s and $\overline{\Delta T} = 23 \pm 1\,^{\circ}\text{C}$), Natural-2 over $t_2 \leq t(\text{min}) \leq t_2+30$ (Table 3, run 18 with $\dot{M}_{\text{in}} \approx 1.30 \pm 0.05$ g/s and $\overline{\Delta T} = 19 \pm 1\,^{\circ}\text{C}$), and Natural-1 Repeated over $t_3 \leq t(\text{min}) \leq t_3+30$ (run 1 repeated). The mass flow rates for these three and other steady state FC cases are plotted along with their $\overline{\Delta T}$ values in Fig. 10. The steady pressures and temperatures measured at different locations along the test section are plotted in Figs. 11(*b*) and Fig. 11(*c*), respectively. Time histories of variations in temperature and pressure of subsystems A, C, and D for the cases in (Figs. 11(*a*)–11(*c*)) are not shown here for brevity but are available in Figs. 12(d)–12(e) of Narain et al. [31].

The FC cases reported in Table 3 lie in a zone bounded by semischematic curves X and Y, as shown in Fig. 10. These bounding curves, at the present moment, are approximate and schematic in nature, as no more than two points on each of the curves have been obtained by experiments or computations. All FC cases in Table 3 and Fig. 10 are category II cases, and the point of FC lies inside the test section (i.e., $X_{\text{FC}} \leq L$ in Fig. 9). This was verified by simulations performed for each of the FC cases. The curve Y (with two computationally obtained points) depicts the right bound on the test matrix. For cases to the right hand side of this curve, the natural point of FC will lie out of the test section and any steady flow that will be realized will belong to the uninvestigated category I cases dealing with specified FC. If the *L*/*V* separator had a natural open vapor outlet (which it does not have because the valve V_3 in Fig. 3 is closed), then curve Y would have represented the transition to partial condensation. Curve X (with two experimentally obtained points), on the left hand side in Fig. 10, represents a system instability that marks a lower left bound on the test matrix. As the mass flow rate decreases below the value given by this curve, there is an experimentally observed instability in the flow, which, in all likelihood, marks the constraining boundary (due to pressure constraints related to saturation pressure in the *L*/*V* separator) representing the limited range of available exit pressures to choose from. It can be seen in Fig. 12 that there exists a steady flow for $\dot{M}_{\text{in}} \approx 1.2$ g/s and 0.8 g/s, but as it is reduced to $\dot{M}_{\text{in}} \leq 0.6$ g/s, the schematic curve X (the suggested boundary between steady annular to unsteady plug/slug) in Fig. 10 is crossed from right to left. The inlet mass flow rate never stabilizes for these cases, but the inlet pressure, as shown in Fig. 12, appears to be less erratic. These transition points are evident, for the circled experimental points on curve X, where unsteadiness/spikes of the type shown in Fig. 12 are observed. These unsteady spikes in the inlet flow rate are probably due to the bridges of the liquid that form across the cross section area when X_{FC} becomes significantly smaller than *L* in Fig. 9 and the desired value of exit pressure falls below the lower bound for allowable exit pressures (the allowed range would typically keep the test-section flow from listening to the downstream vapor pressure restrictions in the *L*/*V* separator). These formations may introduce the observed unsteadiness (Fig. 12) in the inlet mass flow rate and inlet pressure.

Although, at present, different boundaries defined in Figs. 7 and 10 are approximate and schematic, some representative full and partial condensation cases on these boundaries have already been obtained (either by experiments or by computations).

The research outlined in this paper mainly focuses on the inte-

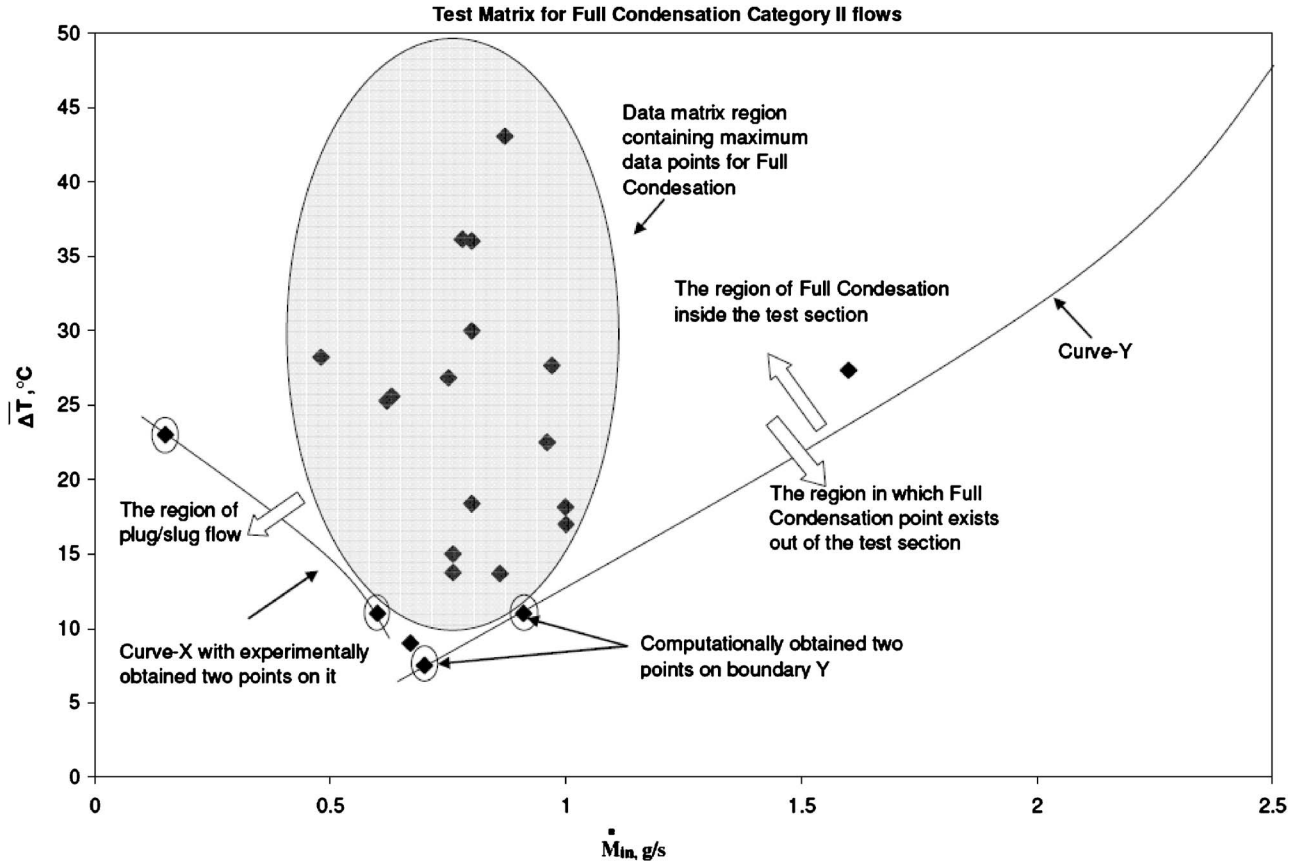

Fig. 10 Two-dimensional test data matrix for category II (unspecified exit-condition) FC case points and different bounding curves represented on the $\dot{M}_{in}-\overline{\Delta T}$ plane

rior region bounded by these curves (see the shaded regions in Figs. 7 and 10), and a careful investigation of the bounding curves and their proper nondimensionalization are a part of future (ongoing) research that awaits more detailed experimental results and better flow visualization.

Even though the exit pressure currently cannot be actively specified for the FC cases, the response of the category II FC cases to disturbances in exit pressure was experimentally ascertained for a number of cases marked in Fig. 10. The exit pressure disturbance was given in the Natural-2 case (see Fig. 11(*a*)) by changing the pressure at the L/V separator (Fig. 3) momentarily. It is seen from Fig. 11(*a*) that although this disturbance died out quickly for the inlet vapor flow rate $\dot{M}_{in}$, the disturbance died out much more slowly for the Δp, which is an indicator of changes in the liquid vapor configuration in the test section. In fact, for all FC cases, the exit pressure disturbance died out in the manner indicated above, showing the generally robust nature of these cases, except for their sensitivity to changes in the exit zone flow variables, as indicated by the Δp response. In fact, even when the aforementioned momentary pressure disturbances in the L/V separator (by injecting liquid through a syringe) was followed by a permanent partial closing of valve V′ in Fig. 3, the same dynamic recovery was observed; however, the recovery time was longer. Also, as seen in Fig. 11(*a*) for the Natural-1 Repeated case, these flows are stable against disturbances in inlet flow rates as well. In this sense, all the category II FC cases in the shaded region of Fig. 10 were found to be robust, pointing to the fact that this experimental procedure is conducive for achieving the steady flow situations associated with the presence of steady attractors for gravity driven condensate flows (see Ref. [1]). It should be noted that the steady flow's robustness is in part a consequence of the appropriate flow loop design whereby the displacement pump P_1 in Fig. 3 continually allows, in the approximate shaded region, the availability of a suitable exit pressure being sought by the flow. This is due to the nature of pump P_1 being "displacement" type and due to its ability to track the inlet mass flow rate $\dot{M}_{in}$. For example, the observed robustness of these fully condensing flows is not at all present in FC cases investigated by others (see, e.g., Ref. [9]) for the earlier described category III flow cases.

4.2.3 Comparisons With Relevant Computational Results (Full Condensation). The simulations for most of the FC cases reported in this paper confirm the fact that the point of FC lies within the test section and almost all the cases lie in the region bounded by the curves X and Y shown in Fig. 10. The simulations performed only up to X_{FC} (with $X_{FC}<L$ in Fig. 9) also predict that the length X_{FC} for FC decreases as the mass flow decreases or the value of ΔT increases. For example, the length of the FC case estimated by the computations for run 11 in Table 3 (with $\dot{M}_{in}\approx 0.97$ g/s and $\overline{\Delta T}=27°C$) is approximately 0.3 m, while that for run 13 in Table 3 (with $\dot{M}_{in}\approx 0.8$ g/s and $\overline{\Delta T}=36°C$) is 0.15 m. The computationally obtained steady and noise-free film thickness and local wall heat-flux values for run 12 in Table 3 (with $\dot{M}_{in}\approx 0.87$ g/s and $\overline{\Delta T}=43°C$) are shown in Fig. 13 over $x\leq X_{FC}$. As seen from Fig. 13, the computationally found length of FC X_{FC} was around 0.2 m. Therefore, results are shown only up to 0.2 m and not up to $L=0.8$ m. As stated earlier, this is because the current simulation methodology cannot simulate the region between X_{FC} and L shown in Fig. 9. Experimental comparisons for these computationally predicted local variations in film thickness and heat-flux values are not currently available but are expected in the near future.

The inclusion of correlations for local or average heat-transfer

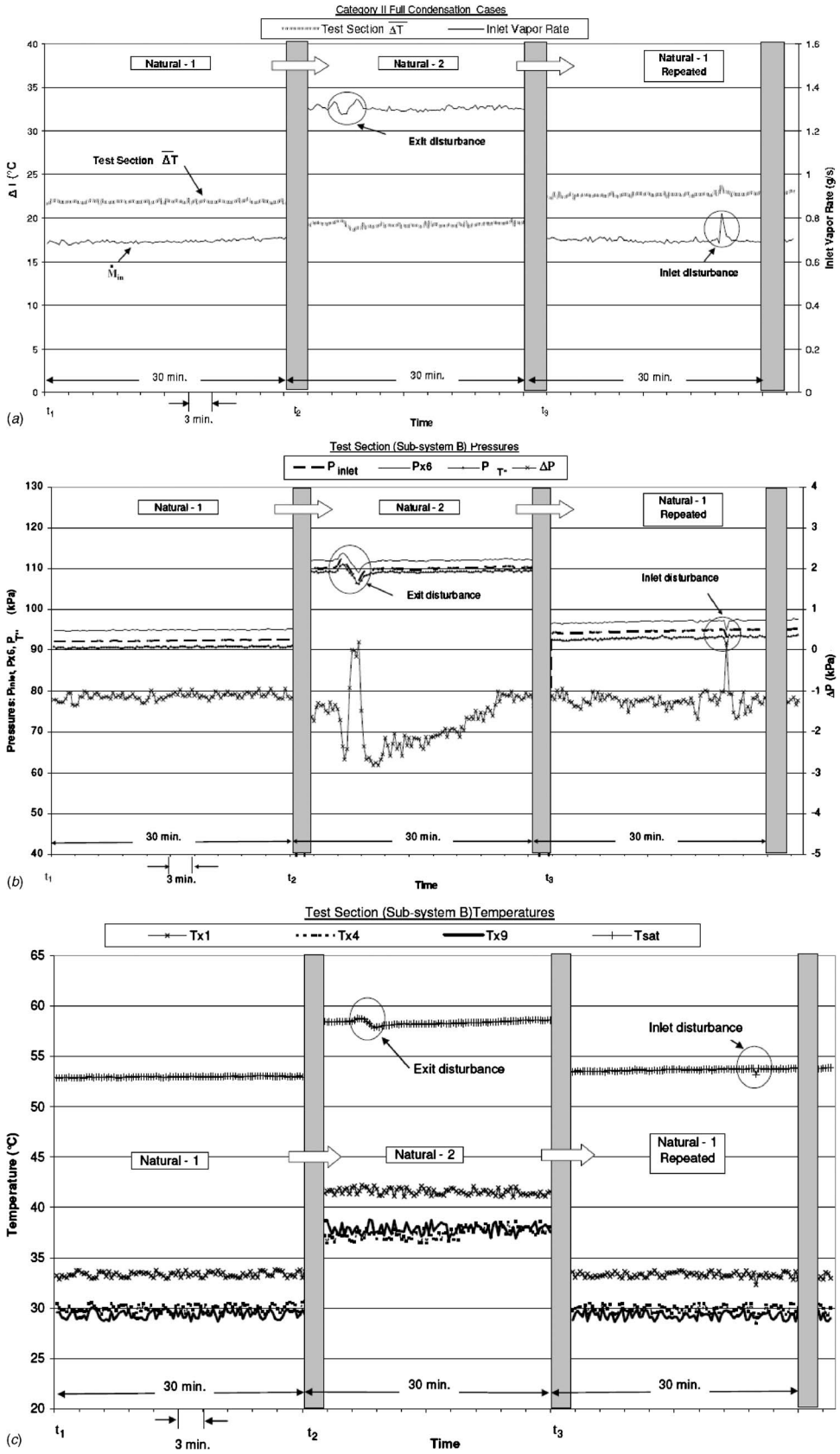

Fig. 11 (*a*) **Time history depiction of $\dot{M}_{in}$ and $\overline{\Delta T}$ values for multiple steady states of FC category II cases, viz., Natural-1 (run 1 from Table 3), Natural-2 (run 18 from Table 3), and Natural-1 Repeated.** (*b*) **Time history of pressures (along and outside the test section) and Δp values for the cases shown in** (*c*) **Time history of temperature values along the test section (subsystem B) for the cases shown in** (*a*).

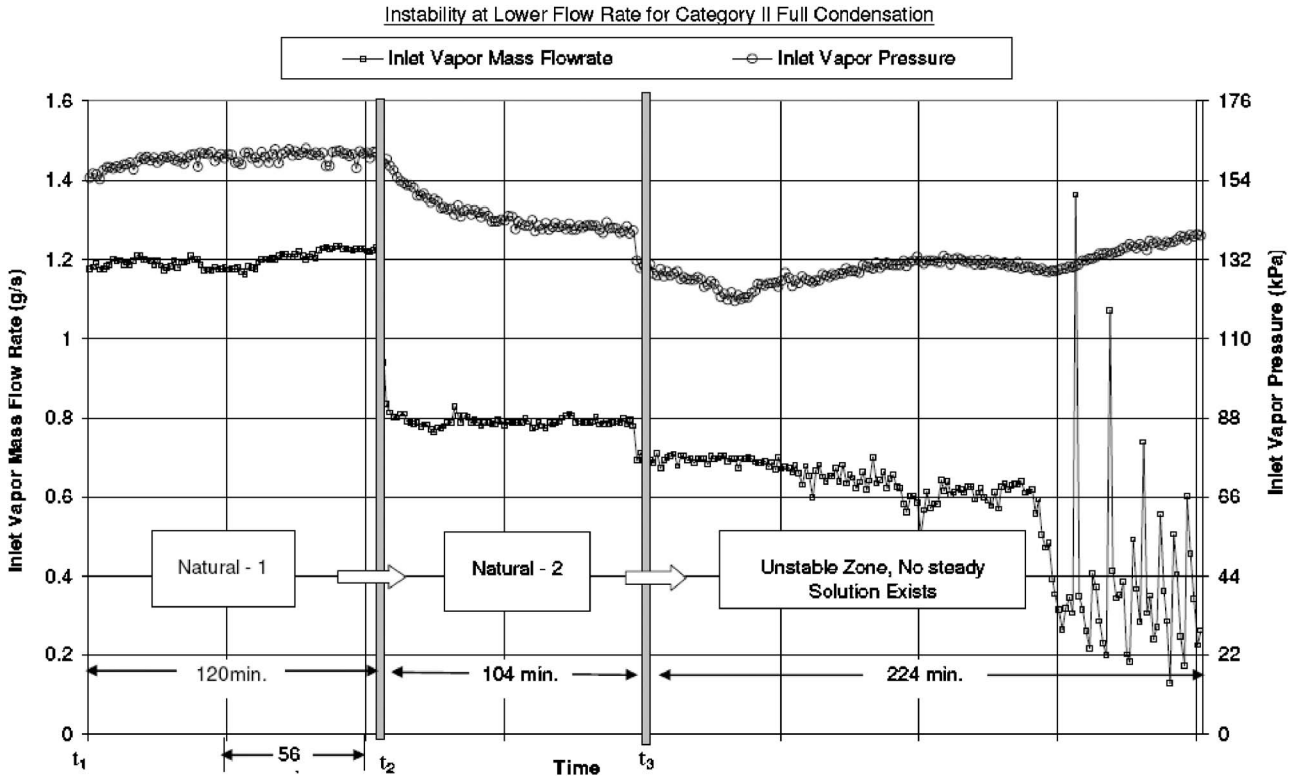

Fig. 12 Time history ($t_3 \leq t\,\text{min} \leq t_3+224$) of mass flow rate and inlet vapor pressure for an attempted unspecified exit-condition (category II) FC case that resulted in instability or transients as the boundary curve X in Fig. 10 is crossed

coefficients is outside the scope of the present paper and is not desirable until a comprehensive synthesis of experimental results and computational results on local film thickness and heat flux becomes available. It should be noted that such data—if obtained without full consideration of the proposed framework of different flow categories, subcategories, and their boundaries—would not be very useful.

5 Results/Comments on Oscillatory System Instabilities

While seeking the natural exit condition for some unspecified exit-condition (category II) partial condensation flows, system instabilities—involving oscillatory flows—of the type shown in Figs. 14(*a*) and 14(*b*) are observed (also see dotted curve A in Fig. 7). The origin of these oscillatory flows appears to be the auxiliary condenser, which sees an approximate category III flow for which, in Fig. 3, the L/V separator is at an approximately fixed high pressure and the merger point P_1' is at an approximately fixed lower pressure. These pressures correspond, respectively, to pressures $p_{\text{tank-in}}$ and $p_{\text{tank-out}}$, which appear in the definition given in Sec. 1 for category III flows. Recall that these fully condensing flows in the auxiliary condenser, unlike the ones studied for the test section, are known (as in Ref. [11]) to become oscillatory under certain conditions. Since details of auxiliary condenser flow data were not obtained (because this component was not the focus of the reported investigations), relating this auxiliary condenser instability to the type of stability boundaries discussed in Ref. [11,13] is outside the scope of this study.

It is clear from Figs. 14(*a*) and 14(*b*) that oscillations in vapor mass flow rate at the exit of the test section impose oscillations on the exit pressure and the pressure drop Δp across the test section, while the inlet vapor mass flow rates remain relatively unaffected. Figure 14(*b*) shows the oscillations in other pressure values and the temperature at the rotameter F_2 (which is nearer to the auxiliary condenser). This, along with the known fact (see Fig. 6 in Ref. [1]) that there is a one to one relation between the exit vapor quality and the exit pressure, indicates an imposition of oscillatory pressures at the exit of the test section.

It suffices here to note that the flow oscillations in the auxiliary condenser can induce an oscillatory exit pressure at the exit of the test-section condenser, and this is the cause, in Figs. 14(*a*) and 14(*b*), of the somewhat reduced level of oscillatory behavior of other test-section flow variables. As a result of the instability in the auxiliary condenser, the dotted curve A in Fig. 7 is merely suggestive of the possible presence of system instabilities. This is because the actual onset of oscillatory conditions has only a very indirect and incomplete relation to the test section $\dot{M}_{\text{in}}$ and $\overline{\Delta T}$ values used in Fig. 7.

The issues regarding the start-up time for the flow loop are discussed in Narain et al. [31] and Kurita [33].

6 Conclusions

This paper experimentally confirms the significance of exit conditions on the nature of quasisteady internal condensing flows and proposes a novel and necessary exit-condition-based categorization of these flows.

In particular, for this gravity driven condensate flow, a way of achieving steady and stable fully condensing flows under unspecified exit-condition cases (category II) is presented. These flows are typically more robust than the fully condensing flows (category III) achieved by a different procedure that has been typically employed and discussed in the existing literature.

The experiments reinforce the simulation results that for partial condensation, multiple steady states, with quite different local and average heat-transfer rates, are often achieved under different exit-condition specifications (category I flows). Therefore, correlations for heat-transfer coefficient (though not developed here) are only meaningful if flow regimes are clearly defined and developed in the framework of proposed exit-condition-based categories.

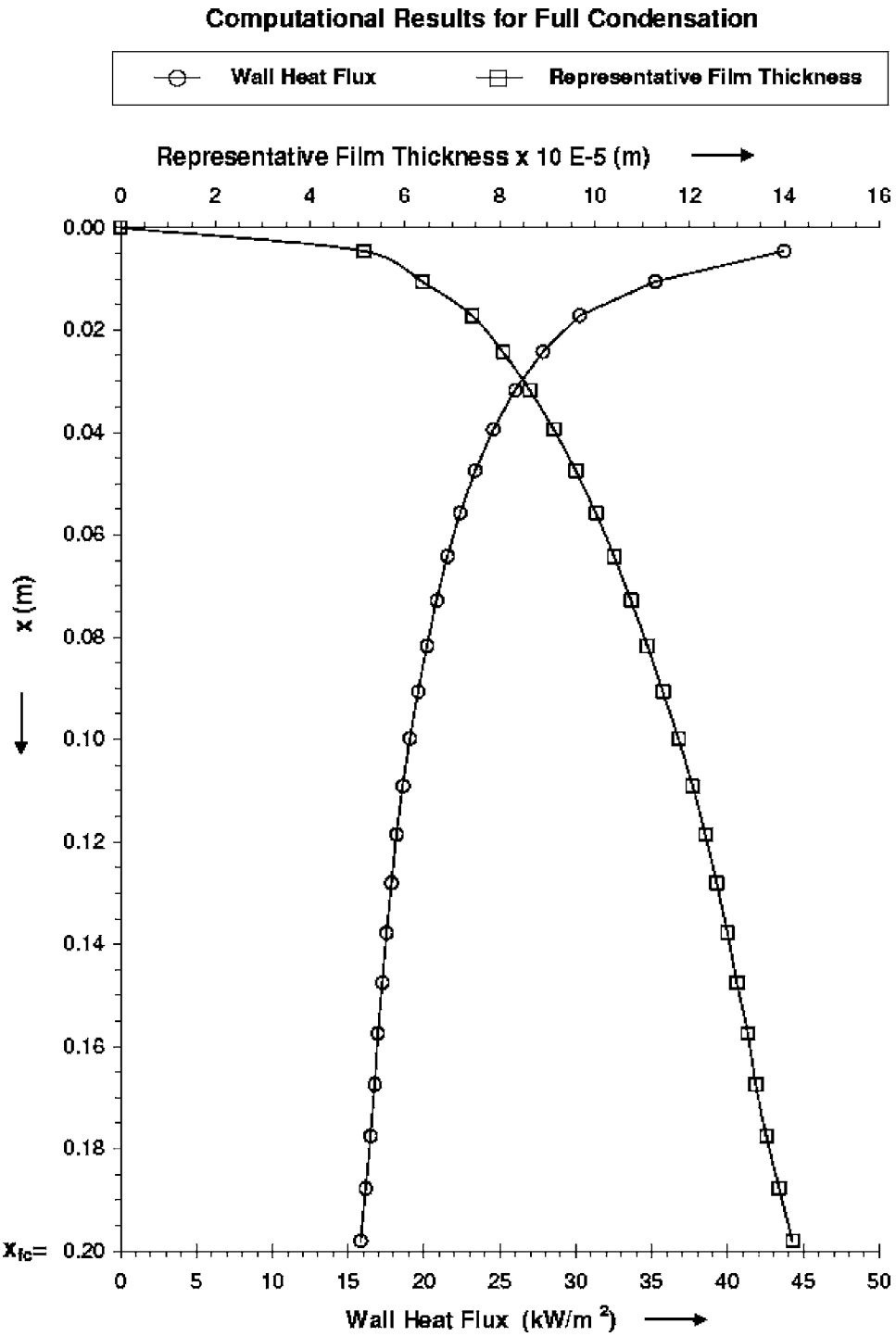

Fig. 13 For a typical category II FC case, this figure shows the computationally obtained representative film thickness and wall heat-flux variation along the test section over $0 \leq x \leq X_{FC}$. The film thickness and heat-flux value shown have been obtained for smooth interface conditions. In fact, they are modulated by waves in the presence of noise (see Ref. [3]). The figure also shows that the length of FC $X_{FC}=0.2$ m is sufficiently shorter than the test-section length L (=0.7 m).

The existing simulation tool's ability to be quantitatively correct in identifying natural exit conditions for gravity driven partial condensation cases under unspecified exit conditions (category II) is very good, as this is supported by the reported experiments. This agreement adds credibility to the experimental results, simulation tool, and the proposed exit-condition-based categorizations.

The transients in partial condensation experiments establish that the steady flows are definitely more robust under the specified exit condition (category I) operation of condensers. This lends credibility to the simulation result that a steady operation of shear driven condensers (in zero gravity and horizontal configurations) is much more difficult to achieve under unspecified exit conditions (category II). In general, these results suggest that all (partial or complete) specified exit-condition flows (category I flows) with

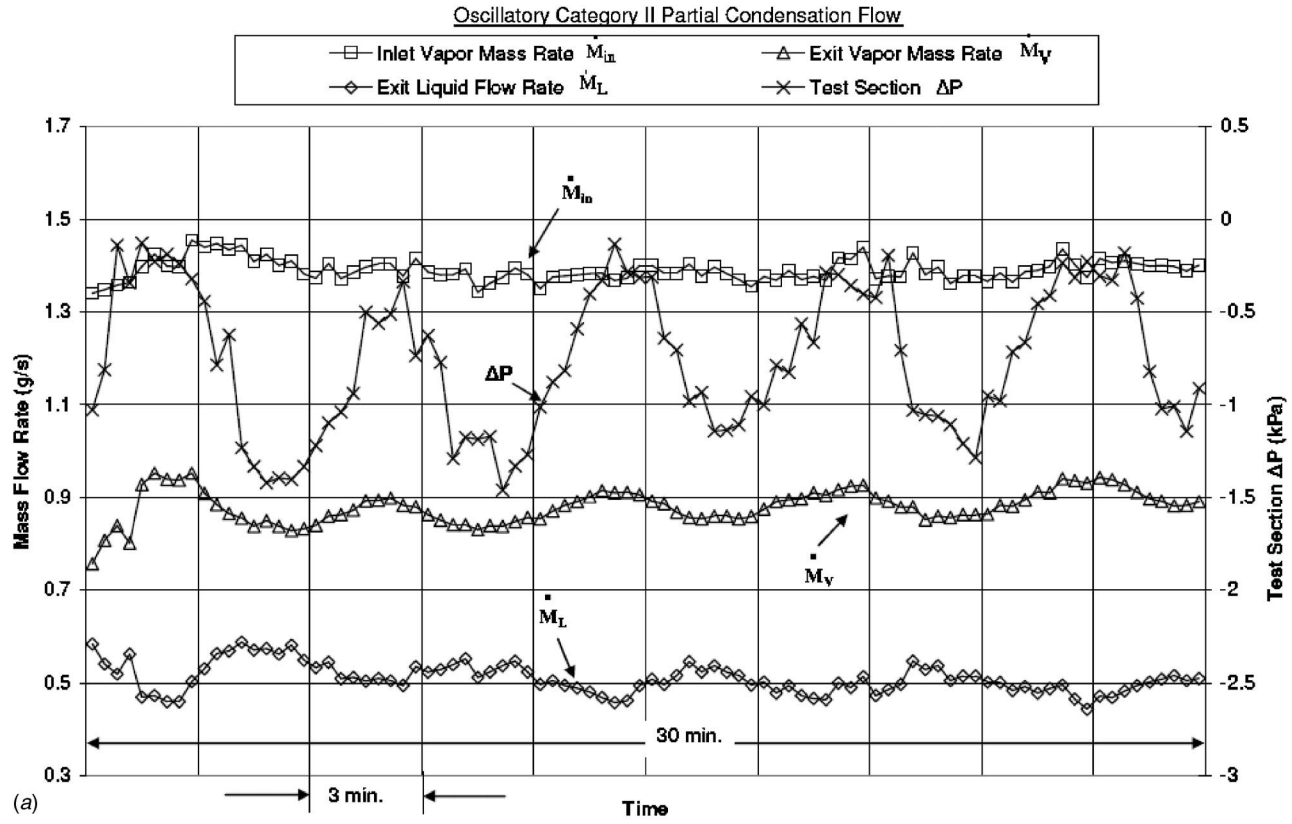

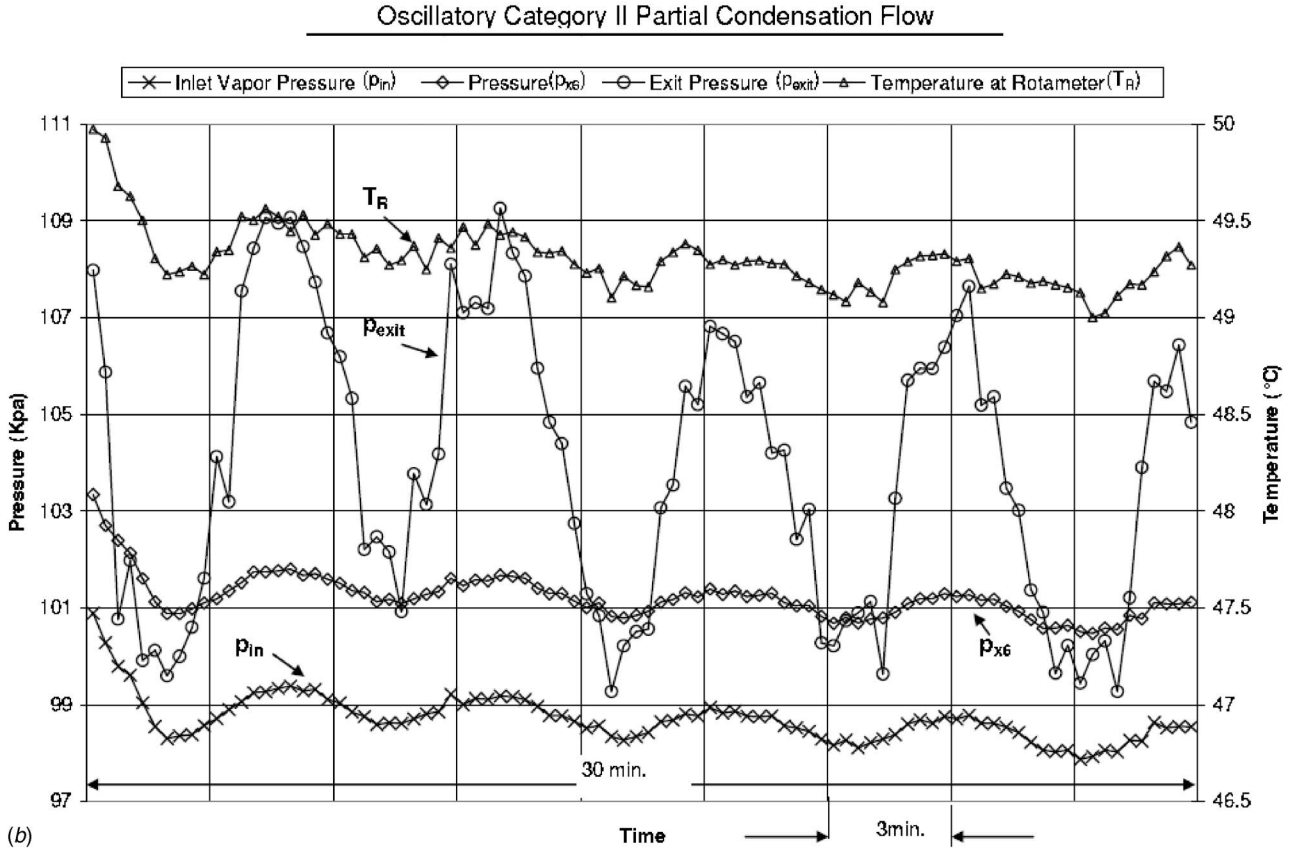

Fig. 14 (*a*) **Time history depiction of $\dot{M}_{in}$, $\dot{M}_V$, $\dot{M}_L$, and Δp values for an oscillatory partial unspecified exit-condition case (category II). In Fig. 7, this flow's appearance is indicated by the crossing of the dotted curve A.** (*b*) **For the case in** (*a*)**, this figure shows the time history depiction of the rotameter temperature T_R and the following pressures: inlet pressure p_{in}, pressure at location 6 in Fig. 5 (p_{x6}), and exit pressure p_{exit}.**

properly selected exit pressure values are likely to be more robust and more readily realized than an operation under other arrangements (category II or category III under arbitrarily fixed pressures and valve settings).

Various flow regime and system boundaries for annular category I and category II flows are observed and reported. Though reported preliminary identifications of flow regime boundaries need to be made more definitive, their identifications are clearly important for attaining or ascertaining steady performances of condensers.

The experiments clearly demonstrate the difference between flow regime boundaries and system-instability boundaries and the importance of identifying system-instability boundaries that are specific to individual systems. For example, curve-A in Fig. 7 and curve-X in Fig. 10 represent system instability boundaries that arise from restrictions imposed on the exit pressure by phenomenon occurring in components downstream of the test section.

Acknowledgment

This work was supported by the NSF Grant No. CTS-0086988 and NASA Grant No. NNC04GB52G.

Nomenclature

$C_p|_L$ = specific heat of the liquid condensate, J/(kg K)
$C_p|_V$ = specific heat of the vapor, J/(kg k)
D = inner diameter of the test-section, m
FC = abbreviation for full condensation
G = inlet mass flux, $4\dot{M}_{\text{in}}/(\pi D^2)$, kg/(m^2/s)
$h_{\text{fg}}(p_{\text{in}})$ = heat of vaporization at pressure p_{in}, J/kg
$\bar{h}$ = average heat-transfer coefficient, $\dot{Q}_{\text{out}}/(\pi DL)$, W/(m^2 K)
Ja = condensate liquid Jakob number, $C_p|_L \cdot \overline{\Delta T}/h_{\text{fg}}(p_{\text{in}})$
$\text{Ja}|_V$ = vapor Jakob number, $C_p|_V \Delta T_{\text{sup}}/h_{\text{fg}}(p_{\text{in}})$
k_L = conductivity of condensate liquid, W/(m K)
L = length of the test section, m
$\dot{M}_{\text{in}}$ = vapor flow rate at test-section inlet, g/s
$\dot{M}_L$ = liquid flow rate at test-section exit, g/s
$\dot{M}_V$ = vapor flow rate at test-section exit, g/s
p_b = evaporator (boiler) pressure, kPa
p_{D2} = pressure at the location near the rotameter, kPa
$p_{T''}$ = pressure at a location downstream of the test section, kPa
p_{in} = pressure at the test-section inlet, kPa
p_{exit} = pressure at the test-section exit, kPa
Pr_1 = condensate liquid Prandtl number, $\mu_{1.} C_p|_L/k_L$
p_{xi} = test-section pressures at different locations $x=xi$ $(i=1,2,\ldots)$, kPa
$\bar{q}''$ = average convective heat flux, W/m^2
$\dot{Q}_b$ = net heat rate into the evaporator, W
$\dot{Q}_{\text{out}}$ = net heat rate out of the test section, W
Re = inlet vapor Reynolds number, $4\dot{M}_{\text{in}}/(\pi D\mu)$
T_b = evaporator fluid temperature, °C
T_R = rotameter fluid temperature, °C
$T_{\text{sat}}(p)$ = saturation temperature at pressure p, °C
$T_{s\text{-}xi}$ = condensing surface temperatures at different locations $x=xi$ $(i=1,2,\ldots)$, °C
$\bar{T}_w$ = mean condensing surface temperature, °C
$T_w(x)$ = nonuniform steady condensing surface temperature, °C
$T_{V\text{-in}}$ = vapor temperature at test-section inlet, °C
$T_{C\text{-in}}$ = temperature of the counter-current coolant water flow at the approach to the test section, °C
x = distance along the test section, m
x_e = ratio of test-section length to test-section inner diameter (L/D).
X_{FC} = approximate length needed for full condensation (estimted by computations), m
$\overline{\Delta T}$ = $T_{\text{sat}}(p)$-$\bar{T}_w$, °C
ΔT_{sup} = vapor superheat, $T_{V\text{-in}}$-$T_{\text{sat}}(p)$ °C
Δp = p_{in}-p_{exit}, kPa
Z_e = ratio of exit vapor mass flow rate to total inlet mass flow rate
$Z(x)$ = ratio of vapor mass flow rate to total mass flow rate at any location x along the test section
ρ_2 = density of vapor, kg/m^3
ρ_1 = density of liquid, kg/m^3
μ_2 = viscosity of vapor, kg/(m s)
μ_1 = viscosity of liquid, kg/(m s)
τ_D = transient decay time for disturbances, s

Subscripts

exit = test-section exit
in = test-section inlet
Na = natural steady case
expt = obtained from experiments
comp = obtained from computations

References

[1] Narain, A., Liang, Q., Yu, G., and Wang, X., 2004, "Direct Computational Simulations for Internal Condensing Flows and Results on Attainability/Stability of Steady Solutions, Their Intrinsic T Waviness, and Their Noise-Sensitivity," J. Appl. Mech., **71**, pp. 69–88.

[2] Liang, Q., Wang, X., and Narain, A., 2004, "Effect of Gravity, Shear and Surface Tension in Internal Condensing Flows—Results From Direct Computational Simulations," ASME J. Heat Transfer, **126**(5), pp. 676–686.

[3] Phan, L., Wang, X., and Narain, A., 2006, "Exit condition, Gravity and Surface-Tension Effects on Stability and Noise Sensitivity Issues for Steady Condensing Flows Inside Tubes and Channels," Int. J. Heat Mass Transfer, **49**(13–14), pp. 2058–2076.

[4] Goodykoontz, J. H., and Dorsch, R. G., 1966, "Local Heat Transfer Coefficients for Condensation of Steam in Vertical Down Flow Within a 5/8-Inch-Diameter Tube," NASA Report No. TN D-3326.

[5] Goodykoontz, J. H., and Dorsch, R. G., 1967, "Local Heat Transfer Coefficients and Static Pressures for Condensation of High-Velocity Steam Within a Tube," NASA Report No. TN D-3953.

[6] Carpenter, F. G., 1948, "Heat Transfer and Pressure Drop for Condensing Pure Vapors Inside Vertical Tubes at High Vapor Velocities," Ph.D thesis, University of Delaware.

[7] Yu, G., 1999, "Development of a CFD Code for Computational Simulations and Flow Physics of Annular/Stratified Film Condensation Flows," Ph.D thesis, ME-EM Department, Michigan Technological University.

[8] Rabas, T. J., and Arman, B., 2000, "Effects of the Exit Condition on the Perofromance of In-Tube Condensers," Heat Transfer Eng., **21**(1), pp. 4–14.

[9] Wedekind, G. L., and Bhatt, B. L., 1977, "An Experimental and Theorotical Investigation in to Thermally Governed Transient Flow Surges in Two-Phase Condensing Flow," ASME J. Heat Transfer, **99**(4), pp. 561–567.

[10] Bhatt, B. L., and Wedekind, G. L., 1980, "Transient and Frequency Characteristics of Two-Phase Condensing Flows: With and Without Compressibilty," ASME J. Heat Transfer, **102**(3), pp. 495–500.

[11] Bhatt, B. L., and Wedekind, G. L., 1980, "A Self Sustained Oscillatory Flow Phenomenon in Two-Phase Condensing Flow Systems," ASME J. Heat Transfer, **102**(4), pp. 695–700.

[12] Wedekind, G. L., and Bhatt, B. L., 1989, "Modeling the Thermally Governed Transient Flow Surges in Multitube Condensing Flow Systems With Thermal Flow Distribution Asymmetry," ASME J. Heat Transfer, **111**(3), pp. 786–791.

[13] Bhatt, B. L., Wedekind, G. L., and Jung, K., 1989, "Effects of Two-Phase Pressure Drop on the Self-Sustained Oscillatory Instabilty in Condensing Flow," ASME J. Heat Transfer, **111**, pp. 538–545.

[14] Boyer, D. B., Robinson, G. E., and Hughes, T. G., 1995, "Experimental Investigation of Flow Regimes and Oscillatory Phenomena of Condensing Steam in a Single Vertical Annular Passage," Int. J. Multiphase Flow, **21**(1), pp. 61–74.

[15] Wedekind, G. L., Kobus, C. J., and Bhatt, B. L., 1997, "Modeling the Characteristics of Thermally Governed Transient Flow Surges in Multitube Two-Phase Condensing Flow Systems With Compressibility and Thermal and Flow Distribution Asymmetry," ASME J. Heat Transfer, **119**(3), pp. 534–543.

[16] Kobus, C. J., Wedekind, G. L., and Bhatt, B. L., 2000, "Predicting the Influence of Compressibility and Thermal and Flow Distribution Asymmetry on the Frequency-Response Characteristics of Multitube Two-Phase Condensing Flow Systems," ASME J. Heat Transfer, **122**(1), pp. 196–200.

[17] Kobus, C. J., 2003, "An Investigation Into the Effect of Subcooled Liquid Inertia on Flowrate Induced Frequency-Response Characteristics of Horizontal

Condensing Flow Systems," *Proceedings of the 6th ASME/JSME Thermal Engineering Joint Conference (AJTEC)*, Hawaii, Mar. 16–23.
[18] Wallis, G. B., 1969, *One-Dimensional Two-Phase Flow*, McGraw-Hill, New York.
[19] Lahey, R. T., and Drew, D. A., 2000, "The Analysis of Two-Phase Flow and Heat Transfer Using A Multidimensional, Four Field, Two-Fluid Model," Nucl. Eng. Des., **204**, pp. 29–44.
[20] Liao, N. S., Wang, C. C., and Tien, C. L., 1988, "Analysis of Transient Flow Surge Phenomena in a Single-Tube Condenser," Int. Commun. Heat Mass Transfer, **15**, pp. 257–268.
[21] Liao, N. S., and Wang, C. C., 1990, "Transient Response Characteristics of Two-Phase Condensing Flows," Int. J. Multiphase Flow, **16**, pp. 139–151.
[22] Wang, C. C., and Liao, N. S., 1989, "Transient Response of a Double-Pipe Condenser to Change of Coolant Flowrate," Int. Commun. Heat Mass Transfer, **16**, pp. 325–334.
[23] Patankar, S. V., 1980, *Numerical Heat Transfer and Fluid Flow*, Hemisphere, Washington, D.C.
[24] Garimella, S., Killion, J. D., and Coleman, J. W., 2002, "An Experimentally Validated Model for Two-Phase Pressure Drop in the Intermittent Flow Regime for Circular Microchannels," J. Fluids Eng., **124**, pp. 205–214.
[25] Garimella, S., Killion, J. D., and Coleman, J. W., 2003, "An Experimentally Validated Model for Two-Phase Pressure Drop in the Intermittent Flow Regime for Non-Circular Microchannels," J. Fluids Eng., **125**, pp. 887–894.
[26] Phan, L., and Narain, A., 2007, "Non-Linear Stability of the Classical Nusselt Problem of Film Condensation and Wave Effects," ASME J. Appl. Mech., **74**, pp. 279–290.
[27] Lu, Q., and Suryanarayana, N. V., 1995, "Condensation of a Vapor Flowing Inside a Horizontal Rectangular Duct," J. Heat Transfer, **117**, pp. 418–424.
[28] Nusselt, W., 1916, "Die Oberflächenkondesation des Wasserdampfes," Z. Ver. Deut. Ing., **60**(27), pp. 541–546.
[29] Palen, J. W., Kistler, R. S., and Frank, Y. Z., 1993, "What We Still Don't Know About Condensation in Tubes," in *Condensation and Condenser Design*, J. Taborek, J. Rose, and I. Tanasawa, eds., United Engineering Trustees, Inc. for Engineering Foundation and ASME, New York, pp. 19–53.
[30] Ng, T. N., 2006, "Development and Calibration of a Fluorescence and Fiber-Optics Based Real-Time Thickness Sensor for Dynamic Liquid Films," Ph.D thesis, MEEM, Michigan Technological University.
[31] Narain, A., Kurita, J. H., Kivisalu, M., Siemionko, A., Kulkarni, S., Ng., T., Kim, N., and Phan, L., 2007, "Internal Condensing Flows Inside a Vertical Pipe—Experimental/Computational Investigations of the Effects of Specified and Unspecified (Free) Exit Conditions at Exit," technical Report, available at http://www.me.mtu.edu/~narain/narainpublications1.htm.
[32] Siemionko, A., 2006, "Design, Fabrication, and Operation of a System to Control FC-72 Condensation Inside a Vertical Tube," Ph.D thesis, Chem. Eng. Michigan Technological University.
[33] Kurita, J. H., 2006, "Experimental Investigation of Fully Condensing Downward Vapor Flows in a Vertical Tube—Unspecified (Free) Exit Condition Cases," M.S. thesis, MEEM, Michigan Technological University.
[34] Parratt, L. G., 1961, *Probability and Experimental Errors in Science: An Elementary Survey*, Wiley, New York.
[35] Carey, V. P., 1992, *Liquid-Vapor Phase-Change Phenomena*, Series in Chemical and Mechanical Engineering, Hemisphere, New York.